

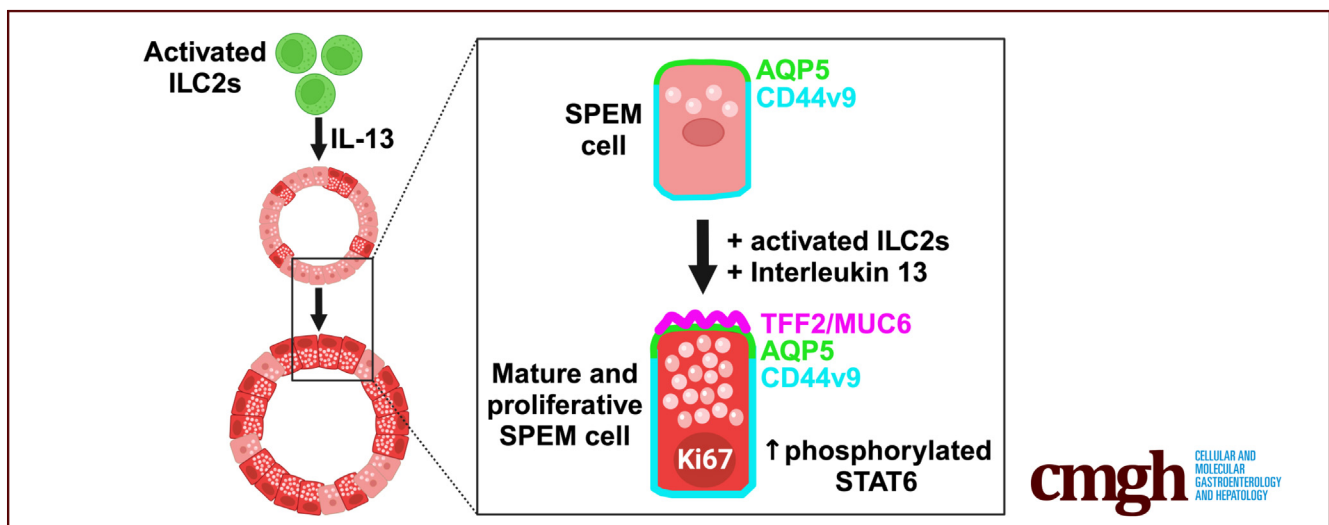
## ORIGINAL RESEARCH

## Interleukin 13 Promotes Maturation and Proliferation in Metaplastic Gastroids



Ela W. Contreras-Panta,<sup>1,2,\*</sup> Su-Hyung Lee,<sup>2,3,\*</sup> Yoonkyung Won,<sup>2,3</sup> Allison E. Norlander,<sup>4</sup> Alan J. Simmons,<sup>1,2</sup> R. Stokes Peebles Jr.,<sup>4,5,6,7</sup> Ken S. Lau,<sup>1,2,3</sup> Eunyoung Choi,<sup>1,2,6</sup> and James R. Goldenring<sup>1,2,3,6,7</sup>

<sup>1</sup>Department of Cell and Developmental Biology, Vanderbilt University, Nashville, Tennessee; <sup>2</sup>Epithelial Biology Center, Vanderbilt University Medical Center, Nashville, Tennessee; <sup>3</sup>Section of Surgical Sciences, Vanderbilt University Medical Center, Nashville, Tennessee; <sup>4</sup>Division of Allergy, Pulmonary and Critical Care Medicine, Vanderbilt University School of Medicine, Nashville, Tennessee; <sup>5</sup>Department of Pathology, Microbiology, and Immunology, Vanderbilt University School of Medicine, Nashville, Tennessee; <sup>6</sup>Department of Medicine, Vanderbilt University School of Medicine, Nashville, Tennessee; and <sup>7</sup>Nashville VA Medical Center, Nashville, Tennessee



## SUMMARY

Type 2 innate lymphoid cells and IL-13 can trigger phosphorylation of STAT6 in SPEM cells. They also promote maturation and proliferation of SPEM cells by increasing production of mucinous proteins.

**BACKGROUND & AIMS:** Type 2 innate lymphoid cells (ILC2s) and interleukin-13 (IL-13) promote the onset of spasmodic polypeptide-expressing metaplasia (SPEM) cells. However, little is known about molecular effects of IL-13 in SPEM cells. We now sought to establish a reliable organoid model, Meta1 gastroids, to model SPEM cells *in vitro*. We evaluated cellular and molecular effects of ILC2s and IL-13 on maturation and proliferation of SPEM cells.

**METHODS:** We performed single-cell RNA sequencing to characterize Meta1 gastroids, which were derived from stomachs of Mist1-Kras transgenic mice that displayed pyloric metaplasia. Cell sorting was used to isolate activated ILC2s from stomachs of IL-13-tdTomato reporter mice treated with

L635. Three-dimensional co-culture was used to determine the effects of ILC2s on Meta1 gastroids. Mouse normal or metaplastic (Meta1) and human metaplastic gastroids were cultured with IL-13 to evaluate cell responses. Air-Liquid Interface culture was performed to test long-term culture effects of IL-13. *In silico* analysis determined possible STAT6-binding sites in gene promoter regions. STAT6 inhibition was performed to corroborate STAT6 role in SPEM cells maturation.

**RESULTS:** Meta1 gastroids showed the characteristics of SPEM cell lineages *in vitro* even after several passages. We demonstrated that co-culture with ILC2s or IL-13 treatment can induce phosphorylation of STAT6 in Meta1 and normal gastroids and promote the maturation and proliferation of SPEM cell lineages. IL-13 up-regulated expression of mucin-related proteins in human metaplastic gastroids. Inhibition of STAT6 blocked SPEM-related gene expression in Meta1 gastroids and maturation of SPEM in both normal and Meta1 gastroids.

**CONCLUSIONS:** IL-13 promotes the maturation and proliferation of SPEM cells consistent with gastric mucosal regeneration.

(*Cell Mol Gastroenterol Hepatol* 2024;18:101366; <https://doi.org/10.1016/j.jcmgh.2024.101366>)

**Keywords:** SPEM; Interleukin-13; STAT6; CD44v9; AQP5; ILC2; Maturation; Proliferation.

Worldwide, gastric cancer remains the fifth most diagnosed cancer and the fourth leading cause of cancer-related deaths.<sup>1,2</sup> It is predicted that these numbers for gastric cancer will increase to around 1.8 million new cases and approximately 1.3 million deaths around the globe by 2040.<sup>3</sup> More than 95% of gastric cancers are known to be adenocarcinomas, and according to the Laurén's classification, they can be categorized into 2 types, diffuse and intestinal. The intestinal-type adenocarcinoma is mostly associated with *Helicobacter pylori* infection and chronic inflammation. As noted previously,<sup>4,5</sup> gastric carcinogenesis develops in the context of 2 different types of metaplastic stages, from pyloric metaplasia to intestinal metaplasia, that ultimately progress to adenocarcinoma. Therefore, it is important to understand the molecular mechanisms behind the maturation and progression of the metaplastic cell lineages that contribute to development of adenocarcinoma.

Using different mouse models, researchers have demonstrated that *H pylori* or *H felis* infection-induced chronic inflammation and loss of parietal cells (oxyntic atrophy) promote the development of pyloric metaplasia.<sup>6-9</sup> Pyloric metaplasia is characterized in the gastric corpus by the presence of glands with an expansion of MUC5AC-expressing foveolar cells toward the lumen, loss of parietal cells, and the replacement of chief cells by the spasmolytic polypeptide-expressing metaplasia (SPEM) cell lineage at the base.<sup>10,11</sup> The replacement of fully mature chief cells occurs by their transdifferentiation into SPEM cells.<sup>12-15</sup> This transdifferentiation is achieved by 3 major steps: first, the activation of autophagy to consume and recycle zymogen granules, and second, the up-regulation of genes related to production of mucus proteins including *Tff2* and *Muc6* that give rise to the mature cell phenotype of SPEM cells. Although transdifferentiation does not require proliferation, after the transition to SPEM lineages, in a third phase, these mucous cells can reenter the cell cycle to expand the mucous metaplastic lineages.<sup>16</sup> Our previous studies revealed that parietal loss initiates transdifferentiation of chief cells. These transitioning cells can be detected by expression of CD44 variant isoform 9 (CD44v9) or Aquaporin 5 (AQP5) before up-regulation of mucinous protein expression.<sup>17</sup> Subsequently, trefoil factor 2 (TFF2)- or mucin 6 (MUC6)-expressing granules appear in the cytosol of transdifferentiating cells, indicative of the mucinous phenotype of mature SPEM cells.<sup>18</sup> SPEM cell lineages can become proliferative after acquiring the mucinous phenotype, which is functionally important for tissue regeneration.<sup>19</sup>

Different studies have shown that there is a strong immune component driving the development of pyloric metaplasia.<sup>20-22</sup> We recently characterized the role of type 2 innate lymphoid cells (ILC2s) in response to mucosal damage in the stomach.<sup>23</sup> ILC2s are known to produce an antigen-


independent immune response in different organs with mucosal lining after damage or infection<sup>24,25</sup> because of the presence of receptors for epithelial cell-derived alarmins including interleukin (IL)-25 and IL-33. The interaction of alarmins with ILC2s can trigger production and release of type 2 cytokines to regulate mucous metaplasia development, macrophage activation, and tissue remodeling in different tissues including the intestine and lung.<sup>26-28</sup> We have shown that mucosal damage induced by acute loss of parietal cells caused a release of IL-33 and an increase of activated ILC2s in the mouse stomach. This effect was not observed in IL-33 knockout mice. In addition, single-cell RNA sequencing (scRNA-seq) revealed a unique transcriptional profile of the ILC2s from stomachs with mucosal injury (activated ILC2s), in comparison with ILC2s from healthy stomachs (non-activated ILC2s), which included increased expression of *Il13*, *Il4*, *Il5*, and *Ramp3* genes. In addition, although IL-33 release can induce production of different cytokines including IL-4 and IL-13, in ILC2s, only the lack of IL-13 prevented the transdifferentiation of chief cells into a SPEM lineage in mice.<sup>29</sup> Because treatment with recombinant IL (rIL)-13 in ST2 (IL-33 receptor) knockout mice reestablished the development of SPEM cells after acute loss of parietal cells, IL-13 can be considered the main effector molecule in the axis of IL-33/ILC2s/IL-13.<sup>29</sup>

IL-13 is a cytokine produced by several cell types including CD4+ Th2 cells, eosinophils, ILC2s, and mast cells.<sup>30</sup> When interacting with its receptor, IL-13 promotes receptor dimerization, which can ultimately trigger phosphorylation of the signal transducer and activator of transcription 6 (STAT6). After STAT6 is phosphorylated, it forms homodimers and translocates into the nucleus where it will bind to DNA to finally regulate gene transcription.<sup>31-33</sup> IL-13 has been proven to directly interact with stomach epithelial cells and up-regulate MUC6 expression.<sup>34</sup> In addition, IL-13 seems to also trigger mucin production in goblet cells from the airway epithelium through activation of STAT6. The IL-13/STAT6 pathway and its role in mucus production remain understudied in stomach epithelial cells.

Over the past decade, organoid models have become more popular in biomedical research/preclinical research because

\*Authors share co-first authorship.

**Abbreviations used in this paper:** ALI, air-liquid interface; AQP5, aquaporin 5; ATF3, activating transcription factor 3; BSA, bovine serum albumin; CD, cluster-of-differentiation; CD44v9, CD44 variant isoform 9; Clu, clusterin; DMEM, Dulbecco modified Eagle medium; FACS, fluorescence-activated cell sorting; GSEA, gene set enrichment analysis; GSII, *Griffonia simplicifolia* lectin II; ILC2, type 2 innate lymphoid cell; IL-13, interleukin 13; MUC6, mucin 6; PBS, phosphate-buffered saline; qRT-PCR, quantitative real-time polymerase chain reaction; rIL, recombinant interleukin; scRNA-seq, single-cell RNA sequencing; SD, standard deviation; SPEM, spasmolytic polypeptide-expressing metaplasia; STAT6, signal transducer and activator of transcription 6; TFF2, trefoil factor 2; 3D, three-dimensional; TROP2, trophoblast antigen 2; UMAP, uniform manifold approximation and projection.

 Most current article

© 2024 The Authors. Published by Elsevier Inc. on behalf of the AGA Institute. This is an open access article under the CC BY-NC-ND license (<http://creativecommons.org/licenses/by-nc-nd/4.0/>).

2352-345X

<https://doi.org/10.1016/j.jcmgh.2024.101366>

they can more effectively model tissue organization and function organs.<sup>35,36</sup> Our group has established mouse stomach epithelial organoids, gastroids, with intestinal metaplasia and dysplasia characteristics from the *Mist1-Kras* mouse model.<sup>37</sup> In this study, we describe the establishment and characterization of a novel *in vitro* mouse gastroid line established from *Mist1-Kras-mTmG* for SPEM, designated *Meta1*. Using this SPEM gastroid line and wild-type normal gastroids, we have demonstrated the effects of ILC2s and IL-13 on the SPEM development and maturation. Furthermore, we have demonstrated that the effects of IL-13 can be mediated by the STAT6 signaling pathway *in vivo* and *in vitro*. Finally, we also demonstrate that IL-13 promotes maturation and mucin protein expression in metaplastic human gastroids. All these data suggest that IL-13 is responsible not only for the initiation of transdifferentiation of chief cells into SPEM cells, but also it is responsible for the maturation and proliferation of SPEM cells *in vitro*.

## Results

### *Meta1* Gastroids Maintain SPEM Characteristics *In Vitro*

*Mist1-Kras* mice display pyloric metaplasia, characterized by the presence of SPEM cells at the base of corpus glands, after 1 month of tamoxifen induction, and it progresses to dysplasia after 4 months of induction.<sup>9</sup> Previously, we have developed and characterized dysplastic gastroids from *Mist1-Kras* mice at 4 months after tamoxifen induction, designated as *Meta4*.<sup>37</sup> H&E and immunofluorescence staining confirmed the presence of pyloric metaplasia and dysplasia at 1 and 4 months, respectively, after tamoxifen induction in the *Mist1-Kras* mouse stomachs (Figure 1A). One-month-induced gastric mucosa contained mature SPEM cells expressing markers including AQP5 and *Griffonia simplicifolia* lectin II (GSII, a surrogate marker for Muc6) at the gland base, whereas 4-month-induced tissue presented cells positive for trophoblast antigen 2 (TROP2), a dysplastic marker (Figure 1A). We have now used *Mist1-Kras-mTmG* mice at 1 month after tamoxifen induction to generate and establish a SPEM-like gastroid line that we have designated as *Meta1* (Figure 1B).

After gland isolation, we maintained *Meta1* gastroids in three-dimensional (3D) culture for up to a week before passaging (Figure 1C). We also cultured the *Meta1* gastroids through multiple passages to assess the maintenance of the SPEM-like phenotype. Using immunofluorescence staining, we observed that *Meta1* gastroids mostly contained immature SPEM cells expressing CD44v9 and AQP5, with a few mature SPEM cells expressing not only CD44v9 and AQP5, but also TFF2, across multiple passages (passage 3 to passage 12) (Figure 1D). These data suggest that the *Meta1* gastroid line solely consists of SPEM lineage cells, although they are not fully matured.

We cultured *Meta1* gastroids for up to 2 weeks and compared their growth patterns with previously established *Meta4* dysplastic gastroids (Figure 2A).<sup>37</sup> *Meta1* gastroids showed a more predominant spherical growth pattern with rare budding formation after 1 and 2 weeks in 3D culture

compared with *Meta4* gastroids, which presented prominent budding formation (Figure 2). Quantitation of budding formation confirmed that *Meta1* gastroids displayed less budding formation in long-term culture when compared with *Meta4* gastroids (Figure 2B). Increased budding formation in *Meta4* gastroids may reflect the potential that dysplastic cells have for irregular epithelial cell stratification and loss of basal cell polarity. Moreover, it could potentially reflect that aggressiveness of dysplastic cells, which is not characteristic of metaplastic cells. In addition, H&E staining showed that *Meta1* gastroids maintain a monolayer conformation until 2 weeks in 3D, whereas *Meta4* gastroids showed multilayering of cells, consistent with the dysplastic organoid phenotype previously reported<sup>37</sup> (Figure 2A). Immunofluorescence staining of gastroids after 2 weeks of 3D culture demonstrated that *Meta1* exhibited a stronger intensity for SPEM cell markers, AQP5 and CD44v9 (Figure 2C). On the other hand, *Meta4* gastroids displayed a weaker intensity for those markers but rather demonstrated strong staining for TROP2, a dysplasia marker (Figure 2C and D).

### *Meta1* Gastroids Display a Differential Transcriptional Profile Compared With Dysplastic Gastroids

We performed scRNA-seq analysis to characterize the *Meta1* transcriptional profile and compare it with *Meta4* gastroid transcriptional profile.<sup>37</sup> Uniform manifold approximation and projection (UMAP) plot showed *Meta1* and *Meta4* have distinct transcriptional profiles (Figure 3A). *Meta1* gastroids were enriched in SPEM-related transcripts including *Tff2*, *Muc6*, *Gkn3*, and *Aqp5* (Figure 3B, top), whereas *Meta4* gastroids expressed dysplasia-related genes like *Mmp7*.<sup>38</sup> Interestingly, *Meta1* gastroid cells expressed chief cell-related genes including *Gif* and *Pgc* (Figure 3B, bottom). This transcriptional background suggests that *Meta1* cells possess transcriptional properties of both transdifferentiating chief cells and SPEM cells.<sup>14</sup>

Differential expression analysis demonstrated the up-regulation of SPEM-related genes and down-regulation of dysplasia-related genes in *Meta1* than in *Meta4* (Figure 3C and D). Unsupervised clustering generated 2 main cell clusters within the *Meta1* gastroids (Figure 3E), Cluster A and Cluster B, and Cluster C, which includes most of the *Meta4* gastroid cells. After gene set enrichment analysis (GSEA), we observed that Cluster B contains genes that are predominant in pathways related to diverse types of epithelial cancers, including gastric cancer (Figure 3F). In addition, metabolic pathways and signaling pathways regulating pluripotency of stem cells were also increased in Cluster B (Figure 3F).

### Mouse-derived ILC2s Co-cultured With *Meta1* Gastroids Promoted Maturation and Proliferation of SPEM Cells in *Meta1* Gastroids

Using a transgenic reporter mouse (IL-13-tdTomato),<sup>39</sup> we induced oxyntic atrophy with L635 treatment, which caused the acute loss of parietal cells and development of pyloric metaplasia in mouse stomach.<sup>40</sup> L635 treatment also induced the infiltration and activation of ILC2s cells



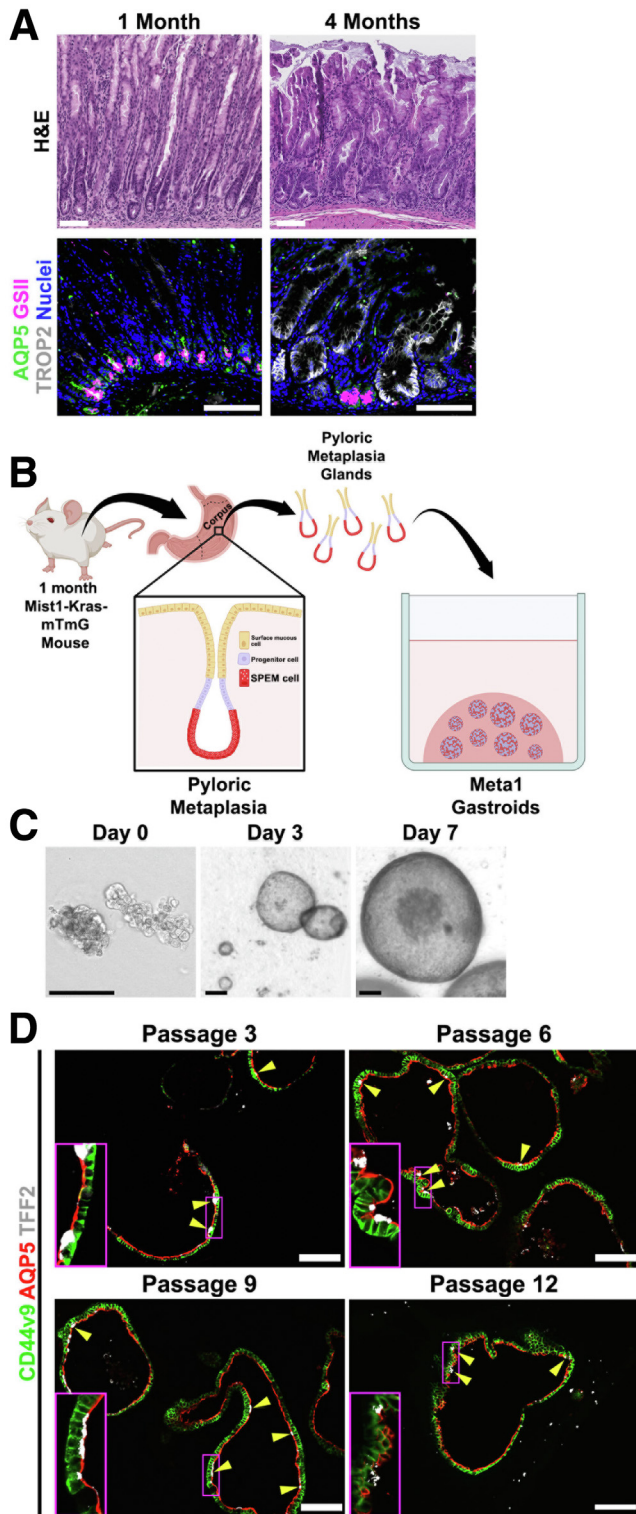


**Figure 1. Establishment and characterization of Meta1 gastroid lines.** (A) H&E staining shows the stomach mucosa used for the generation of the Meta1 and Meta4 gastroids displaying pyloric metaplasia and dysplasia, respectively. Immunofluorescence staining for SPeM cell markers (AQP5 and GSII) and a dysplastic marker (TROP2). Scale bar: 50  $\mu$ m. (B) Schematic illustration of the gastroid establishment process from Mist1-Kras transgenic mice. (C) Representative bright field images of Meta1 gastroids captured at day 0, 3,

reflected in the significant increase of GATA3 and tdTomato double-positive cells (Figure 4A). The stomachs were removed and processed to obtain single cells for cell sorting (Figure 4B). Fluorescence-activated cell sorting (FACS) according to tdTomato expression confirmed an increase of ILC2s in L635-treated mouse stomachs, compared with untreated stomachs (Figure 3C). Sorted tdTomato+ ILC2s were co-cultured with Meta1 gastroids. Live microscopy corroborated the coexistence of GFP+ Meta1 gastroids and activated ILC2s (tdTomato+) in the 3D co-culture (Figure 4D). After 5 days of culture, we observed a significant increase in the growth of co-cultured gastroids, compared with gastroids alone (Figure 4D). Because ILC2s release IL-13, which stimulates STAT6 phosphorylation in other organs,<sup>33</sup> we assessed STAT6 phosphorylation in co-cultures of gastroids with ILC2s. Immunoblotting demonstrated that STAT6 was highly phosphorylated in Meta1 gastroids co-cultured with IL-13-expressing ILC2s compared with Meta1 gastroids only (Figure 4E).

Importantly, immunofluorescence staining demonstrated that in co-culture conditions, Meta1 gastroids had significantly increased numbers of mature SPeM cells double positive for TFF2 and AQP5 (Figure 5A). In addition to the increment of mature SPeM cells, we also observed a significant increase of proliferation of MUC6 and CD44v9 double positive mature SPeM cells (Figure 5B).

### Meta1 Gastroids Had a Stronger Response to IL-13 Than to IL-4

When activated, ILC2s can release type 2 cytokines including IL-4 and IL-13.<sup>28</sup> Both cytokines trigger phosphorylation of STAT6 in different cell types.<sup>41</sup> We studied the response of Meta1 gastroids to these 2 recombinant cytokines. Meta1 gastroids treated with either vehicle (bovine serum albumin [BSA]) or rIL-4 did not show a significant difference in gastroid growth during treatment (Figure 6A). However, quantitation of diameters at different days demonstrated significantly increased sizes in rIL-13-treated Meta1 gastroids starting at day 2 compared with BSA or rIL-4 (Figure 6A). Meta1 gastroids showed an increase in phosphorylation of STAT6 when treated with either rIL-4 or rIL-13; however, the phosphorylation ratio was significantly higher with rIL-13 (Figure 6B). Therefore, we proceeded to investigate the IL-13 effects in Meta1 gastroids.

### IL-13 Promoted Maturation and Proliferation of SPeM Cells in Meta1 Gastroids

We analyzed the cellular effects of IL-13 in the Meta1 gastroids. As seen before, IL-13 promoted growth of individual gastroids in comparison with BSA (Figure 7A, left and

and 7 days after plating. Scale bars: 50  $\mu$ m for first picture and 100  $\mu$ m for second and third. (D) Immunofluorescence staining of Meta1 gastroids cross sections for SPeM markers (CD44v9, AQP5, and TFF2). Yellow arrows and enlarged sections indicate presence of mature SPeM cells triple positive for CD44v9, AQP5, and TFF2 in cells. Scale bar: 100  $\mu$ m.

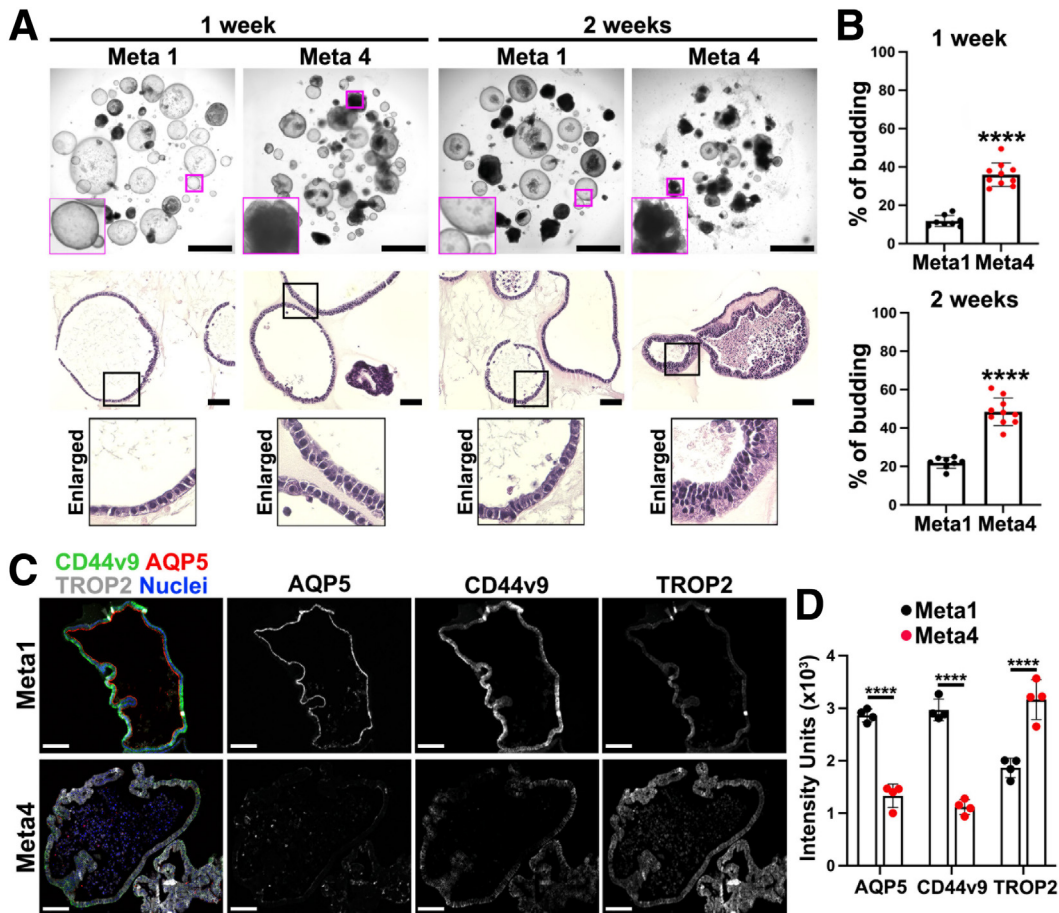


**Figure 2. Meta1 and Meta4 mouse gastroids displayed different behavior.** (A) *Top*, representative bright field images of Matrigel domes containing Meta1 and Meta4 gastroids at 1 or 2 weeks after plating. Scale bar: 500  $\mu\text{m}$ . *Bottom*, H&E staining shows cellular distribution in the Meta1 and Meta4 gastroids. Enlarged images show cellular organization (mono- or multi-layering). Scale bar: 100  $\mu\text{m}$ . (B) Quantitation of the average percentage of gastroids presenting budding formation in Meta1 and Meta4 gastroids at 1 or 2 weeks of *in vitro* culture. Mean  $\pm$  SD (N= 8–10 from 3 independent experiments). \*\*\*\* $P < .0001$ . (C) Immunofluorescence staining of Meta1 and Meta4 gastroids after 2 weeks of *in vitro* 3D culture for SPEM cell markers (CD44v9 and AQP5) and a dysplastic cell marker (TROP2). Scale bar: 100  $\mu\text{m}$ . (D) Quantitation of intensity units for different SPEM and dysplastic cell markers in gastroids on C. Mean  $\pm$  SD (n = 4). \*\*\*\* $P < .0001$ .

right). After daily following of the growth of individual gastroids, we observed that the significantly increased diameters started after 2 days of treatment, and it continued augmenting throughout the treatment course. After 4 days of treatment, H&E staining showed that rIL-13-treated Meta1 gastroid cells presented higher cell heights when compared with control gastroids (Figure 7A, middle). We assessed phosphorylation of STAT6 at 4 days of treatment. As observed before, rIL-13 induced STAT6 phosphorylation in Meta1 gastroids compared with control (Figure 7B, left) in a dose-dependent manner (Figure 7B, right). Furthermore, immunofluorescence staining of Meta1 gastroids demonstrated that treatment with rIL-13 increased the number of mature SPEM cells, which were double positive for either TFF2 and AQP5 (Figure 7C) or MUC6 and CD44v9 (Figure 7D, left bar graph). We also observed a significant increase in proliferative SPEM cells (Figure 7D, right bar graph), as seen in Meta1 gastroids co-cultured with ILC2s. All these data together imply that IL-13 alone is enough to

activate STAT6 in Meta1 gastroid cells and to promote the increase of mature and proliferative SPEM cells.

### Two-Dimensional Long-Term Culture of Meta1 Gastroid Cells Exposed to rIL-13 Showed Increased Mucin Production

Air-Liquid Interface (ALI) culture technique was used to expose Meta1 gastroid cells to rIL-13 for an extended time period (Figure 8A). Meta1 gastroids cultured with rIL-13 showed a higher accumulation of mucins depicted as a tenacious mucus layer on the top of the Meta1 gastroid cells after a total of 28 days of ALI when compared with the control (BSA) (Figure 8B). The accumulation of mucins was confirmed through immunofluorescence staining. GSII, a lectin that binds sugars from MUC6, and CD44v9 positive cells were increased after long-term treatment with rIL-13 (Figure 8C). Quantitation of GSII-expressing area per total area corroborated a significant increase in the rIL-

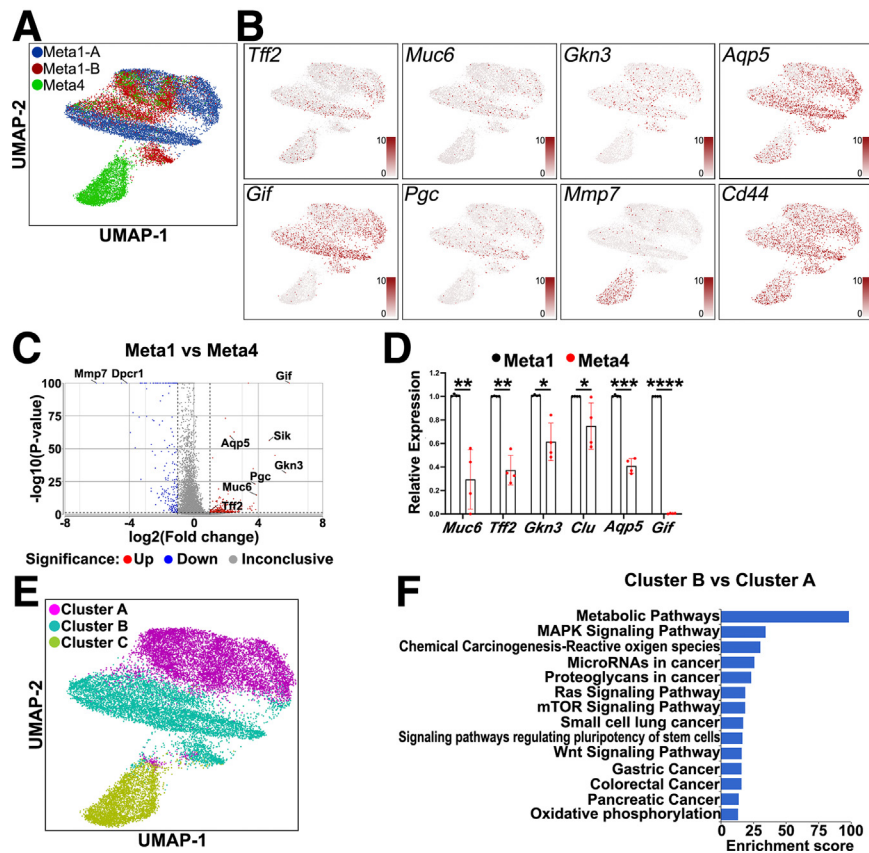


**Figure 3. Single-cell RNA-seq of Meta1 gastroid lines.** (A) UMAP plot three-colored to show the cell distribution of the Meta1 and Meta4 gastroid lines. Each dot represents a single cell. (B) UMAP plots showing expression of different genes in red. *Tff2*, *Muc6*, *Gkn3*, and *Aqp5* are SPEM-related genes and overlaid with Meta1 gastroid-derived cells. *Gif* and *Pgc* are genes expressed in chief cells and overlaid with Meta1 gastroid-derived cells. *Mmp7*, a dysplastic marker, overlaid with the Meta4 gastroid-derived cells and *Cd44* was present in both types of gastroids. (C) Volcano plot of the differentially expressed genes between both Meta1 lines versus Meta4 gastroid line with emphasis in up-regulation of SPEM-related genes and down-regulation of dysplastic-related genes in Meta1 gastroid cells. (D) Quantitative RT-PCR showing the relative expression levels of key chief cell and SPEM cell genes. Mean  $\pm$  SD (n = 4). \* $P < .05$ , \*\* $P < .01$ , \*\*\* $P < .001$ , \*\*\*\* $P < .0001$ . (E) UMAP plot three-colored to show the clusters found in the gastroid lines. There are 2 distinctive cell clusters present in the Meta1 gastroid-derived cells, Cluster A and Cluster B. Cluster C contains most of Meta4 gastroid cells. (F) Gene set enrichment analysis of the Kyoto Encyclopedia of Genes and Genomes database using the up-regulated genes in Cluster B versus Cluster A.

13-treated Meta1 gastroid cells. These data suggest that rIL-13 promotes the maturation of SPEM cells and might be important for maintaining the mucinous phenotype of SPEM cell lineages.

### IL-13-Treated Gastroids Derived From Normal Mice Exhibited the Presence of Mature SPEM Cells

To evaluate the effect of IL-13 on normal gastroids, we isolated normal corpus glands from untreated wild-type stomachs and generated normal gastroids *in vitro*. These gastroids were treated with either rIL-13 or BSA (Figure 9A). After 4 days of treatment, there was no difference in gastroid growth between the 2 groups. However, rIL-13-treated normal gastroids displayed morphologic differences with less spherical shapes (Figure 9B, left). H&E staining showed that rIL-13 treatment induced higher cell heights in the normal gastroids compared with the control

(Figure 9B, right). In accordance with this finding, immunofluorescence staining demonstrated that rIL-13-treated normal gastroids exhibited a significant increase of SPEM cell lineages double positive for AQP5 and MUC6, compared with BSA-treated normal gastroids (Figure 9C). These data confirm the previous results from Noto et al<sup>34</sup> in normal mouse gastroids and suggest that exposure to rIL-13 *in vitro* promotes transdifferentiation of chief cells. Moreover, the increase in expression of MUC6 in cells could explain the increase in cell height because the mucins can accumulate in the cytoplasm under the apical side of mature SPEM cells (Figure 9B).

We further isolated corpus glands from wild-type mice treated with L635 for 3 consecutive days to compare IL-13 treatment in normal gastroids with gastroids prepared from SPEM-containing mucosa *in vivo*. Immunofluorescence staining demonstrated that rIL-13-treated normal gastroids were phenotypically similar to the gastroids generated from acutely injured glands of L635-treated



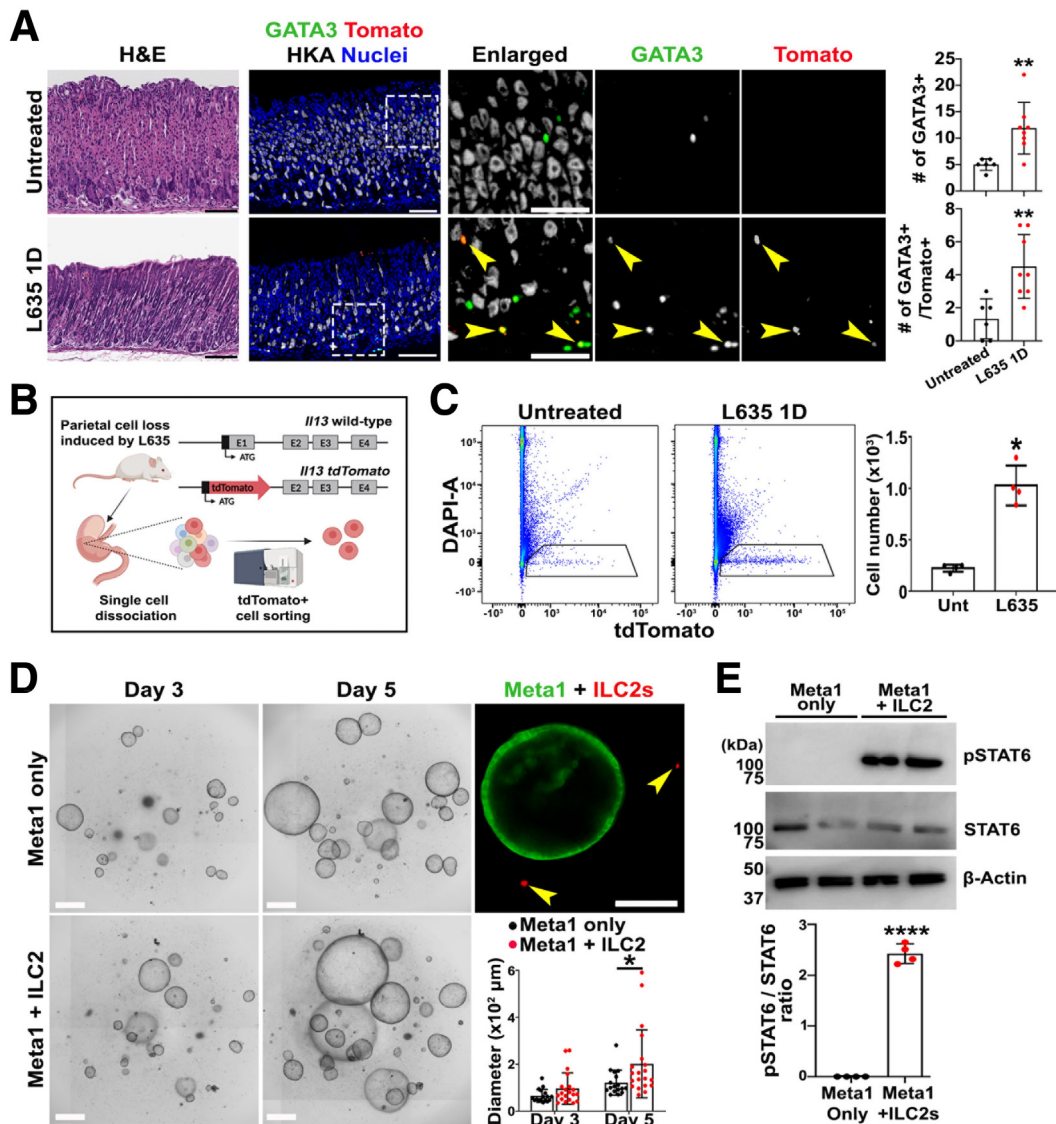


**Figure 4. Isolation of activated ILC2s and 3D co-culture with Meta1 gastroids.** (A) H&E and immunofluorescence staining of stomach tissues from untreated and L635-treated mice. Yellow arrows point to ILC2 cells double positive for GATA3 and TdTomato. Quantitation of GATA3 positive cells (ILC2s) and GATA3 and TdTomato double-positive cells (activated ILC2s). Scale bar: 100 μm. Mean ± SD (n = 6–8 from 3 different experiments). \*\**P* < .01. (B) Schematic illustration of activated ILC2s isolation from L635-treated mice using FACS. (C) FACS plots showing tdTomato positive cells (ILC2s) in untreated and L635-treated mice. Cell number quantitation shows significant increase of tdTomato positive cells (activated ILC2s) in stomachs from treated mice. Mean ± SD (N = 4). \**P* < .05. (D) Representative bright field images of Matrigel domes containing Meta1 gastroids only or co-cultured with ILC2s. Immunofluorescence imaging shows proximity of activated ILC2s (IL-13-tdTomato positive) to the Meta1 gastroid (GFP-positive membrane). Quantitation of gastroid diameters demonstrates significantly higher sizes in Meta1 gastroids co-cultured with ILC2s compared with gastroids only after 5 days of plating. Scale bar: 500 μm. Mean ± SD (N = 4 independent experiments). \**P* < .05. (E) Immunoblotting shows significant up-regulation of phosphorylated STAT6 in Meta1 gastroid co-cultured with ILC2s. Mean ± SD (N = 4 independent experiments). \*\*\*\**P* < .0001.

mice, based on the observations that both presented an increased number of mature SPEM cells double positive for MUC6 and CD44v9 in comparison with BSA-treated normal gastroids (Figure 9D). In addition, immunoblotting showed a significantly higher phosphorylation ratio of STAT6 in rIL-13-treated normal gastroids that was dose-dependent with concentrations higher than 3 ng/mL (Figure 9E). These data together suggest that IL-13 alone can initiate transdifferentiation and complete maturation

of SPEM cells *in vitro* in normal gastroids and mimic the accumulation of MUC6 in gastroids from L635-treated mice (Figure 9F).

We next sought to assess whether IL-13 induction of transdifferentiation into SPEM reflects up-regulation of an antral developmental profile. We performed immunofluorescence staining of normal gastroids and Meta1 gastroids treated with either BSA (untreated) or rIL-13 for MIST1, a mature chief cell marker, and PDX1, which is specifically

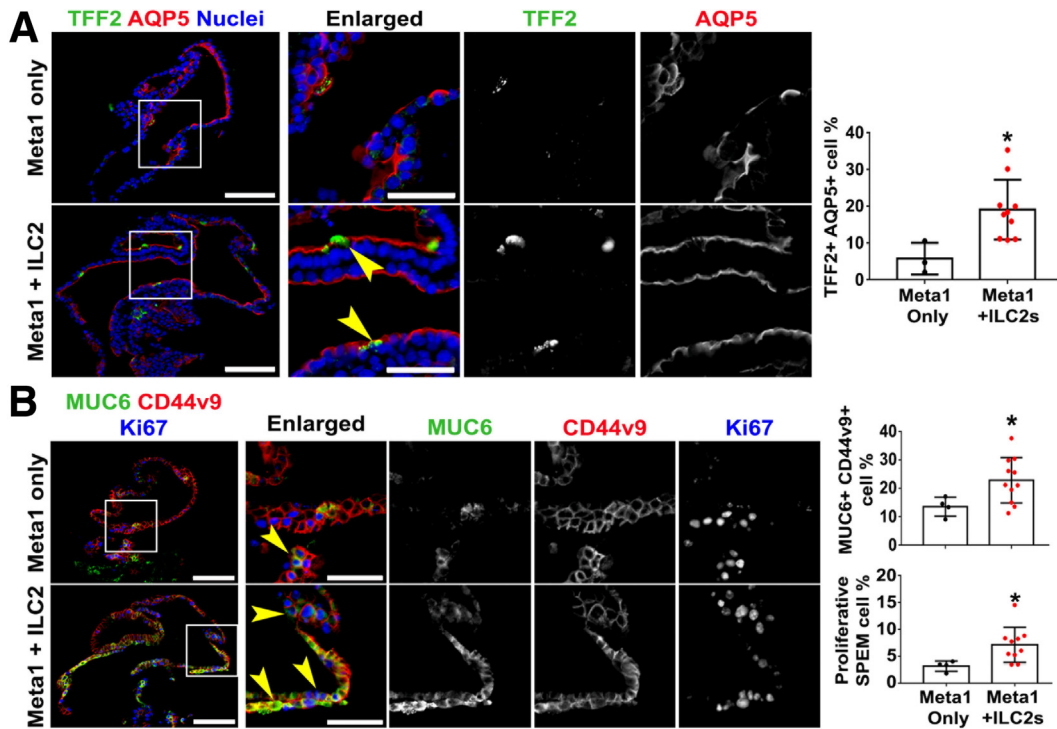


**Figure 5. Co-culture with activated ILC2s promoted maturation and proliferation of SPEM cells in Meta1 gastroids.** (A) Immunofluorescence staining of Meta1 gastroids cross sections for SPEM-related markers, AQP5 and TFF2. Quantitation of AQP5 and TFF2 double positive cells demonstrated significant increase of proportion of mature SPEM cells in co-cultured condition. *Yellow arrowheads* point at double positive mature SPEM cells. Scale bar: 100  $\mu$ m and 50  $\mu$ m for enlarged. Mean  $\pm$  SD (N = 3 independent experiments). \**P* < .05. (B) Immunofluorescence staining of Meta1 gastroids cross sections for a proliferation marker, Ki67, and SPEM-related markers, MUC6 and CD44v9. Quantitation of MUC6 and CD44v9 double positive cells demonstrated significant increase of proportion of mature SPEM cells in Meta1 gastroids co-cultured with ILC2s. Quantitation of MUC6, CD44v9, and Ki67 triple positive cells demonstrated significant increase of proportion of proliferative SPEM cells. *Yellow arrowheads* point at triple positive mature and proliferative SPEM cells. Scale bar: 100  $\mu$ m and 50  $\mu$ m for enlarged. Mean  $\pm$  SD (N = 3 independent experiments). \**P* < .05.

expressed in the antrum but not in the corpus of the stomach. Untreated normal gastroids were composed of a significant number of chief cells that were positive for MIST1 but negative for CD44v9, whereas PDX1 expression was not observed (Figure 10). rIL-13 treatment to normal gastroids increased the proportion of PDX1 positive cells with or without MIST1 expression, indicating IL-13 can indeed cause cell lineage transition from the corpus to the antrum phenotype as well as inducing morphologic changes (Figure 10). Cells of Meta1 gastroids, derived from pyloric metaplastic glands in the corpus, were completely negative for MIST1 but strongly expressed PDX1. These data suggest that normal gastroids and Meta 1 gastroids respond similarly to IL-13.

### STAT6 Can Regulate the Expression of SPEM-related Genes and ATF3

STAT6 can act as a transcription factor to regulate gene expression when it is phosphorylated. Phosphorylated STAT6 can be translocated to the nucleus and recognize a DNA motif with a consensus sequence of 5'-TTCN<sub>4</sub>GAA-3',<sup>32</sup> where N<sub>4</sub> symbolizes a spacer of 4 nucleotides of any type found in DNA (Figure 11A). To investigate further the

mechanism of phosphorylated STAT6 action in promoting maturation of SPEM cells, we predicted putative binding sites for STAT6 in SPEM-related genes using the motif recognition tool from the JASPAR database.<sup>42</sup> Intriguingly, at least 2 positions for binding sites (P1-P2) were found in the upstream promoter region (2000 base pair) of the Transcription Start Site of SPEM-related genes including *Muc6*, *Tff2*, *Gkn3*, *Cd44*, *Wfdc2* (*He4*), and *Atf3* (Figure 11B). In addition, using quantitative real-time-polymerase chain reaction (qRT-PCR), we corroborated the transcriptional up-regulation of *Muc6*, *Tff2*, *Gkn3*, *Cd44v9*, and *Wfdc2* (*He4*). We observed a significant increase in the relative expression of those genes after IL-13 treatment (Figure 11C). The protein level of ATF3 was also significantly increased in the Meta1 gastroids treated with rIL-13 (Figure 11D). These data suggest that STAT6 could promote SPEM cell development and maturation at the transcriptional level.

### Inhibition of STAT6 Attenuated Maturation of SPEM Cells

Because we observed a link between STAT6 phosphorylation and up-regulation of SPEM-related genes, we performed inhibition assays to block STAT6 function *in vitro*. We



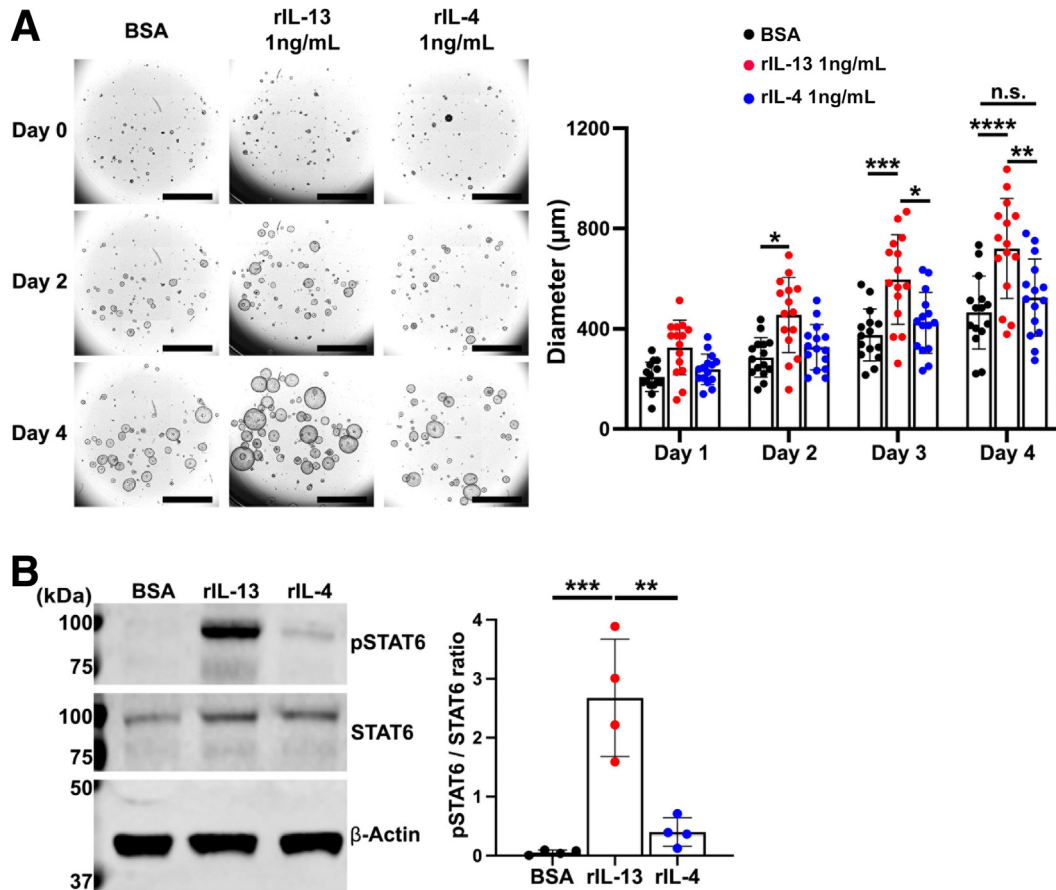


**Figure 6. IL-13 caused higher phosphorylation ratio of STAT6 than IL-4 in Meta1 gastroids.** (A) Representative bright field images of Matrigel domes containing Meta1 gastroids treated with rIL-13, rIL-4, or vehicle solution (BSA). Quantitation of gastroid diameters showed significantly higher sizes in Meta1 gastroids treated with rIL-13 compared with rIL-4 and BSA starting at 2 days of treatment. There was no significant difference between rIL-4- and BSA-treated Meta1 gastroids. Scale bar: 1000  $\mu\text{m}$ . Mean  $\pm$  SD (N = 4 independent experiments). \* $P < .05$ , \*\* $P < .01$ , \*\*\* $P < .001$ , \*\*\*\* $P < .0001$ . (B) Immunoblotting shows significant up-regulation of phosphorylated STAT6 in Meta1 gastroids treated with rIL-13 when compared with rIL-4 and BSA. Mean  $\pm$  SD (N = 4 independent experiments). \*\* $P < .01$ , \*\*\* $P < .001$ .

used a STAT6-specific inhibitor, AS1517499, that blocks STAT6 phosphorylation.<sup>43</sup> AS1517499 was added to IL-13-treated Meta1 gastroids for up to 4 days (Figure 12A). We observed that addition of a STAT6 inhibitor significantly decreased Meta1 gastroid growth after 4 days of treatment (Figure 12B). After performing qRT-PCR, we corroborated the transcriptional down-regulation of *Muc6*, *Tff2*, *Gkn3*, *Cd44v9*, *Atf3*, and *Wfdc2* (*He4*) in Meta1 gastroids treated with both rIL-13 and AS1517499, compared with rIL-13 alone (Figure 12C). Moreover, ATF3 protein levels were also significantly decreased with AS1517499 (Figure 12D).

We next assessed STAT6 inhibition in normal gastroids. AS1517499 was added to IL-13-treated normal gastroids for up to 6 hours (Figure 13A). Immunoblotting for phosphorylated STAT6 revealed a decrease of STAT6 protein and its phosphorylation starting after 1 hour of the AS1517499 addition, and the effect was maintained for up to 6 hours (Figure 13B). In addition, immunofluorescence staining showed that AS1517499 addition caused a significant decrease in MUC6 expression in rIL-13-treated normal gastroids in comparison with rIL-13 alone (Figure 13C). Notably,

AQP5 expression did not change between treatments (Figure 13C), which suggests that STAT6 may regulate mucin production to promote the maturation of SPEM cells.

Finally, we examined STAT6 inhibition in a mouse model of acute oxyntic atrophy. We treated wild-type mice with L635 for 3 days in combination with AS1517499. Corpus mucosa from mice treated with L635 alone showed significantly up-regulated phosphorylation of STAT6 compared with untreated tissue (Figure 14A), as well as increased expression of SPEM-related markers including SOX9 and AQP5 (Figure 14A). In contrast, mice treated with both L635 and AS1517499 did not display a significant up-regulation of either phosphorylated STAT6 or expression of SOX9 (Figure 14A). Consistent with previous results, immunostaining for SPEM markers demonstrated that L635-induced parietal cells loss results in pyloric metaplasia development characterized by SPEM cells at the gland base, which are double positive for GSII and AQP5 (Figure 14B). However, inhibition of STAT6 suppressed the expression of either AQP5 or GSII at the base of fundic glands of mice treated with L635, although the extent of parietal cell loss

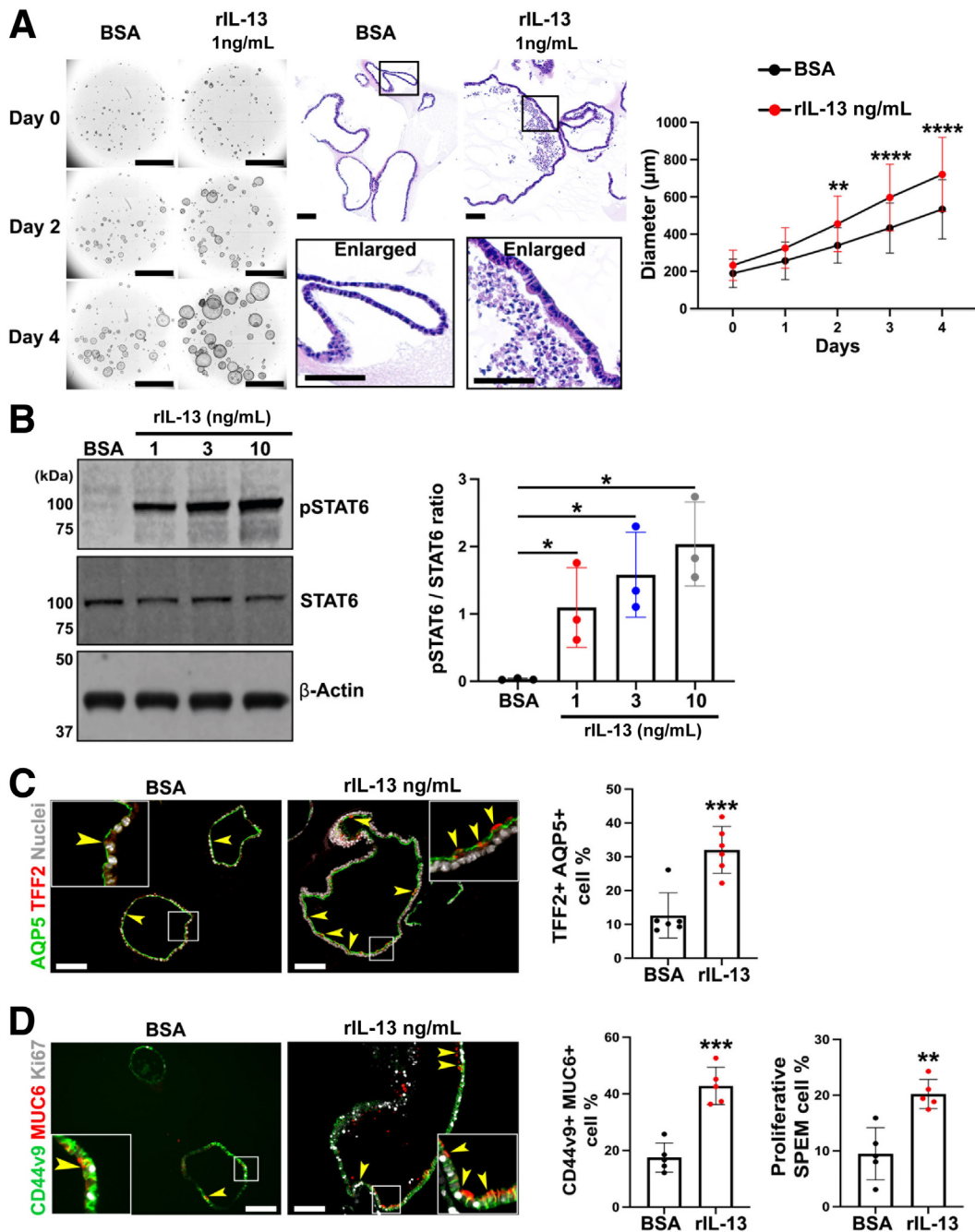


**Figure 7. IL-13 alone promoted phosphorylation of STAT6 and maturation and proliferation of SPEM cells.** (A) Representative bright field images of Matrigel domes containing Meta1 gastroids treated with either rIL-13 or vehicle solution (BSA). Enlarged images from H&E staining show cellular distribution and height differences between the rIL-13-treated and the BSA-treated Meta1 gastroids. Quantitation of matched gastroid diameters showed significantly higher sizes in Meta1 gastroids treated with rIL-13 compared with control after 2 days of treatment. Scale bar: 1000  $\mu$ m for brightfield and 100  $\mu$ m for H&E. Mean  $\pm$  SD (N = 3 independent experiments). \*\* $P$  < .01, \*\*\*\* $P$  < .0001. (B) Immunoblotting shows significant up-regulation of phosphorylated STAT6 in Meta1 gastroids treated with different concentrations of rIL-13 when compared with BSA. Quantitation showed rIL-13-dose-dependent increase. Mean  $\pm$  SD (N = 3 independent experiments). \* $P$  < .05. (C) Immunofluorescence staining of Meta1 gastroids cross sections for SPEM-related markers, AQP5 and TFF2. Quantitation of AQP5 and TFF2 double positive cells demonstrated significant increase of proportion of mature SPEM cells in rIL-13-treated Meta1 gastroids. Yellow arrowheads point at double positive mature SPEM cells. Scale bar: 100  $\mu$ m. Mean  $\pm$  SD (N = 3 independent experiments). \*\*\* $P$  < .001. (D) Immunofluorescence staining of Meta1 gastroids cross sections for a proliferation marker, Ki67, and SPEM-related markers, MUC6 and CD44v9. Quantitation of MUC6 and CD44v9 double positive cells demonstrated significant increase of proportion of mature SPEM cells in rIL-13-treated Meta1 gastroids. Moreover, quantitation of MUC6, CD44v9, and Ki67 triple positive cells demonstrated significant increase of proportion of proliferative SPEM cells. Yellow arrowheads point at triple positive mature and proliferative SPEM cells. Scale bar: 100  $\mu$ m. Mean  $\pm$  SD (N = 3 independent experiments). \*\* $P$  < .01, \*\*\* $P$  < .001.

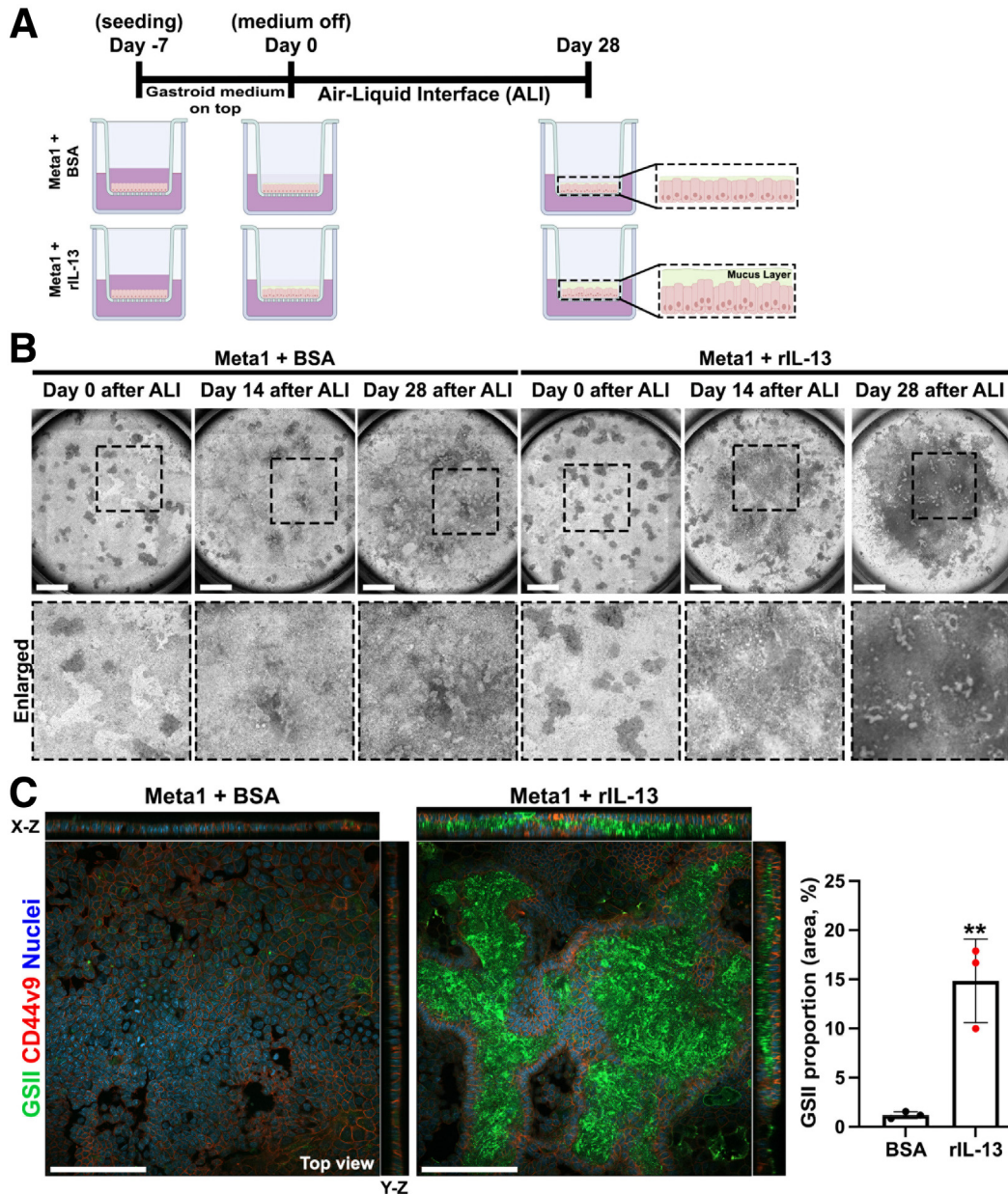


**Figure 8.** IL-13 maintained the mature SPEM phenotype in Meta1 gastroid cells in long-term ALI culture. (A) Schematic illustration of ALI culture procedure. (B) Representative bright field images of top view of ALI filters. Secretion and accumulation of mucins increase after 14 days of culture with rIL-13. At day 28, there was a tenacious mucus layer on top of the Meta1 gastroid cells that were treated with rIL-13. Scale bar: 200  $\mu\text{m}$ . (C) Whole mount immunofluorescence staining for SPEM-related markers, GSII and CD44v9, showed significant increase of GSII coverage proportion in the rIL-13 treatment. Scale bar: 100  $\mu\text{m}$ . Quantitation of GSII staining per cell area is shown on the right. Mean  $\pm$  SD (N = 3 independent experiments).  $^{**}P < .01$ .

was similar to the corpus mucosa treated with L635 alone (Figure 14B). These data suggest that STAT6 activation is necessary for induction of SPEM after acute oxyntic atrophy.

### IL-13 Promoted Maturation and Proliferation of SPEM Cells in Human Metaplastic Gastroids

We analyzed the cellular effects of human rIL-13 in human metaplastic gastroids that were previously established.

These human metaplastic gastroids mostly display SPEM cell markers.<sup>44</sup> As observed in mouse SPEM gastroids (Meta1), IL-13 promoted growth of individual human metaplastic gastroids in comparison with control (BSA) (Figure 15A). We observed a significant increase in the diameters of IL-13-treated human metaplastic gastroids beginning after 5 days of treatment. After a week of treatment, we assessed phosphorylation of STAT6. rIL-13 induced a significant increase in STAT6 phosphorylation ratio in human metaplastic gastroids compared with control



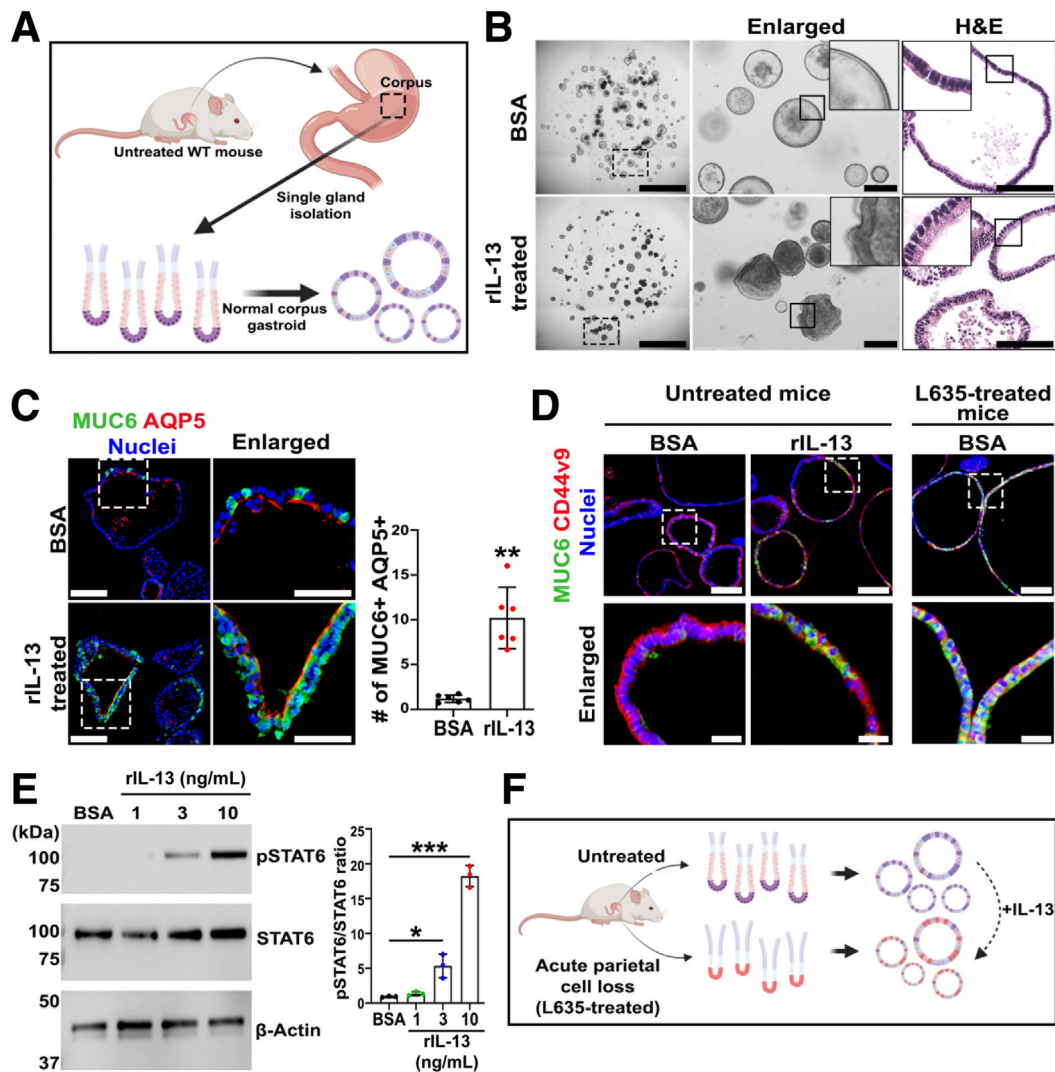


**Figure 9. IL-13 promoted maturation of SPEM cells in normal gastroids and mimicked gastroids derived from L635-treated mice.** (A) Schematic illustration of gland-derived gastroids from untreated wild-type mice. (B) Representative bright field images of Matrigel domes containing normal gastroids cultured with either rIL-13 or vehicle (BSA). Enlarged images show distinct cell heights of the gastroid cell layer. H&E staining shows cell organization and height differences between rIL-13-treated and BSA-treated normal gastroids. Scale bar: 100  $\mu\text{m}$ . (C) Immunofluorescence staining normal gastroids cross sections for SPEM-related markers, MUC6 and AQP5. Quantitation of MUC6 and AQP5 double positive cells demonstrated significant increase of proportion of mature SPEM cells in rIL-13-treated normal gastroids. Scale bar: 100  $\mu\text{m}$  and 50  $\mu\text{m}$  for enlarged. Normalized with gastroid area. Mean  $\pm$  SD (N = 3 independent experiments).  $^{**}P < .01$ . (D) Immunofluorescence staining for SPEM-related markers, MUC6 and CD44v9, of normal gastroids treated with BSA (left), or with rIL-13 (middle), and of gastroids derived from L635-treated mice (right). rIL-13-treated normal gastroids and L635-treatment derived gastroids showed similarities in increased expression of MUC6 when compared with BSA-treated normal gastroids. (E) Immunoblotting shows significant up-regulation of phosphorylated STAT6 in rIL-13-treated normal gastroids compared with BSA. Quantitation showed rIL-13-dose-dependent increase. Mean  $\pm$  SD (N = 3 independent experiments).  $^{*}P < .05$ ,  $^{***}P < .001$ . (F) Schematic illustration of gland-derived gastroids from untreated and L365-treated wild-type mice. Exposure of normal gastroids to rIL-13 promoted the transdifferentiation and maturation toward a SPEM cell phenotype as seen in gastroids derived from mucosa with pyloric metaplasia after L635 treatment.

(Figure 15B). Furthermore, immunofluorescence staining demonstrated that treatment with rIL-13 increased the number of mature SPEM cells, which were double positive for MUC6 and CD44v9 (Figure 15C, top bar graph). We also noted a significant increase in proliferative SPEM cells (Figure 15C, bottom bar graph), as observed in Meta1 gastroids co-cultured with ILC2s or with rIL-13 alone. All these data together indicate that IL-13 alone can activate STAT6

even in human metaplastic gastroid cells and promote the increase of mature and proliferative SPEM cells.

## Discussion

Organoid models have proved to be reliable *in vitro* models to mimic cellular and physiological functions of organ-like structures. They have gained popularity in

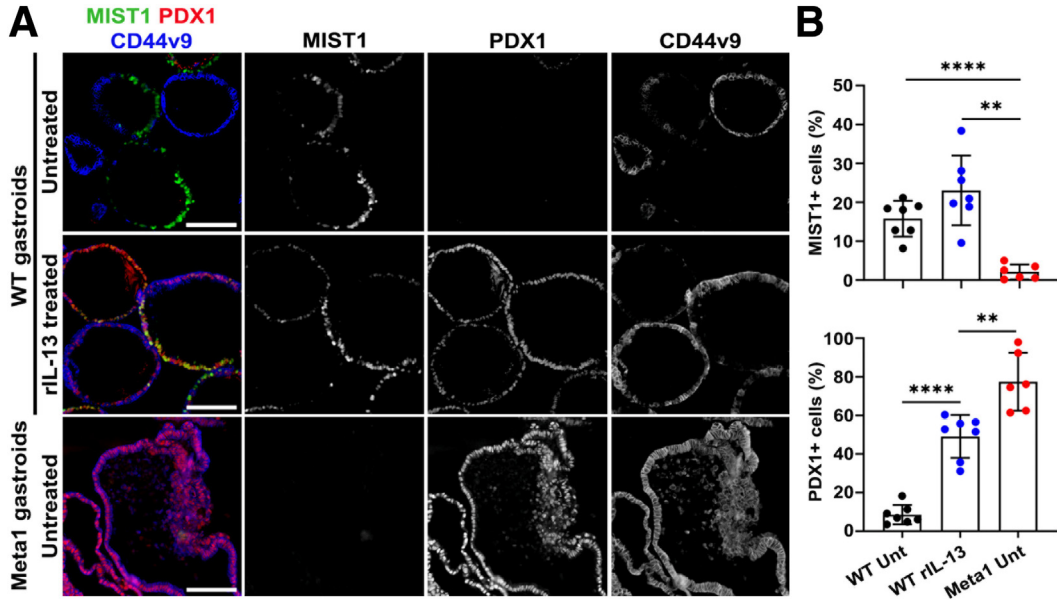


**Figure 10.** rIL-13–treated normal gastroids displayed both chief cell and SPEM cell markers. (A) Immunofluorescence staining for MIST1 (chief cell), PDX1 (an antral lineage marker), and CD44v9 (SPEM cell) in normal gastroids and Meta1 gastroids. Scale bar: 100  $\mu$ m. (B) Quantitation of average percentage of MIST1-positive cells and PDX1-positive cells. Mean  $\pm$  SD (N = 6–7 from 3 independent experiments). \*\* $P < .01$ , \*\*\* $P < .001$ .

personalized medicine because patient-derived organoids are a powerful platform to test treatments and understand disease pathophysiology.<sup>45</sup> In the stomach, a number of groups have used organoid lines to study different stages of stomach carcinogenesis including metaplasia, dysplasia, and adenocarcinoma.<sup>37,46–49</sup> Organoids are an appealing

approach for modeling the development, progression, and behavior of pre-neoplastic stages of cancer. Here we have established a novel gastric organoid (gastroid) line from the stomach corpus with characteristics of pyloric metaplasia, termed Meta1. Meta1 gastroids represent an *in vitro* model of SPEM with expression of CD44v9 and AQP5 as well as

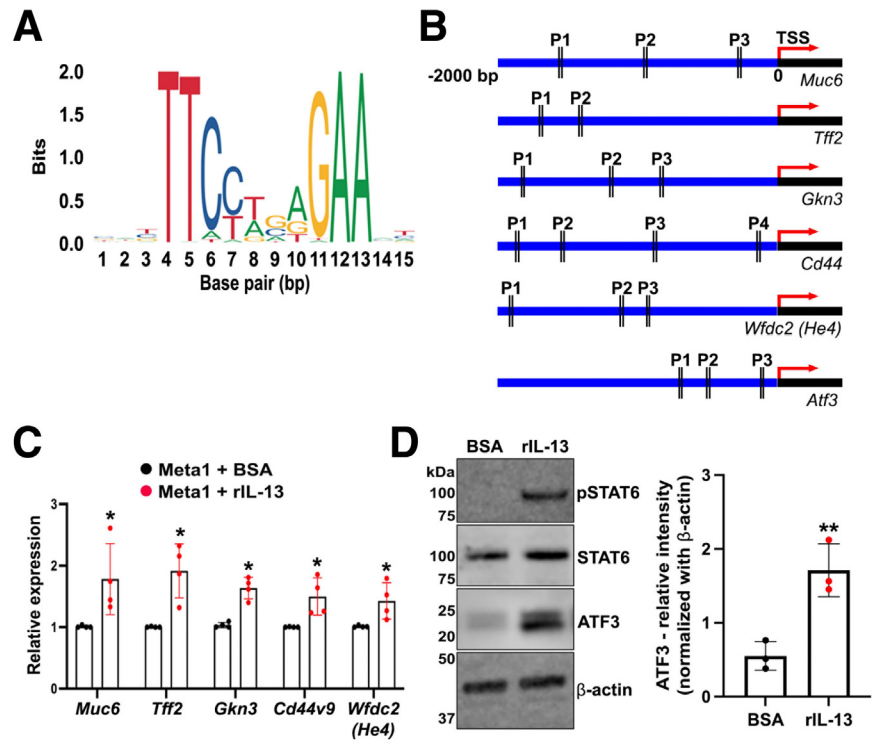


**Figure 11.** STAT6 can up-regulate transcription of SPEM-related genes and the protein expression of ATF3. (A) Consensus sequence of the DNA motif recognized by STAT6. (B) Positions (P1-P4) of the STAT6 binding sites predicted with the JASPAR database.<sup>42</sup> These sites were located upstream -2000 base pairs of the Transcription Start Site (TSS) of SPEM-related genes including *Muc6*, *Tff2*, *Gkn3*, *Cd44*, *He4*, and *Atf3*. (C) Quantitative RT-PCR showing the relative expression levels of SPEM-related genes (*Muc6*, *Tff2*, *Gkn3*, *Cd44v9*, and *He4*). Mean  $\pm$  SD (n = 4 independent experiments). \* $P < .05$ . (D) Immunoblotting shows significant up-regulation of ATF3 protein in Meta1 gastroids treated with rIL-13 compared with vehicle (BSA). Mean  $\pm$  SD (N = 3 independent experiments). \*\* $P < .01$ .

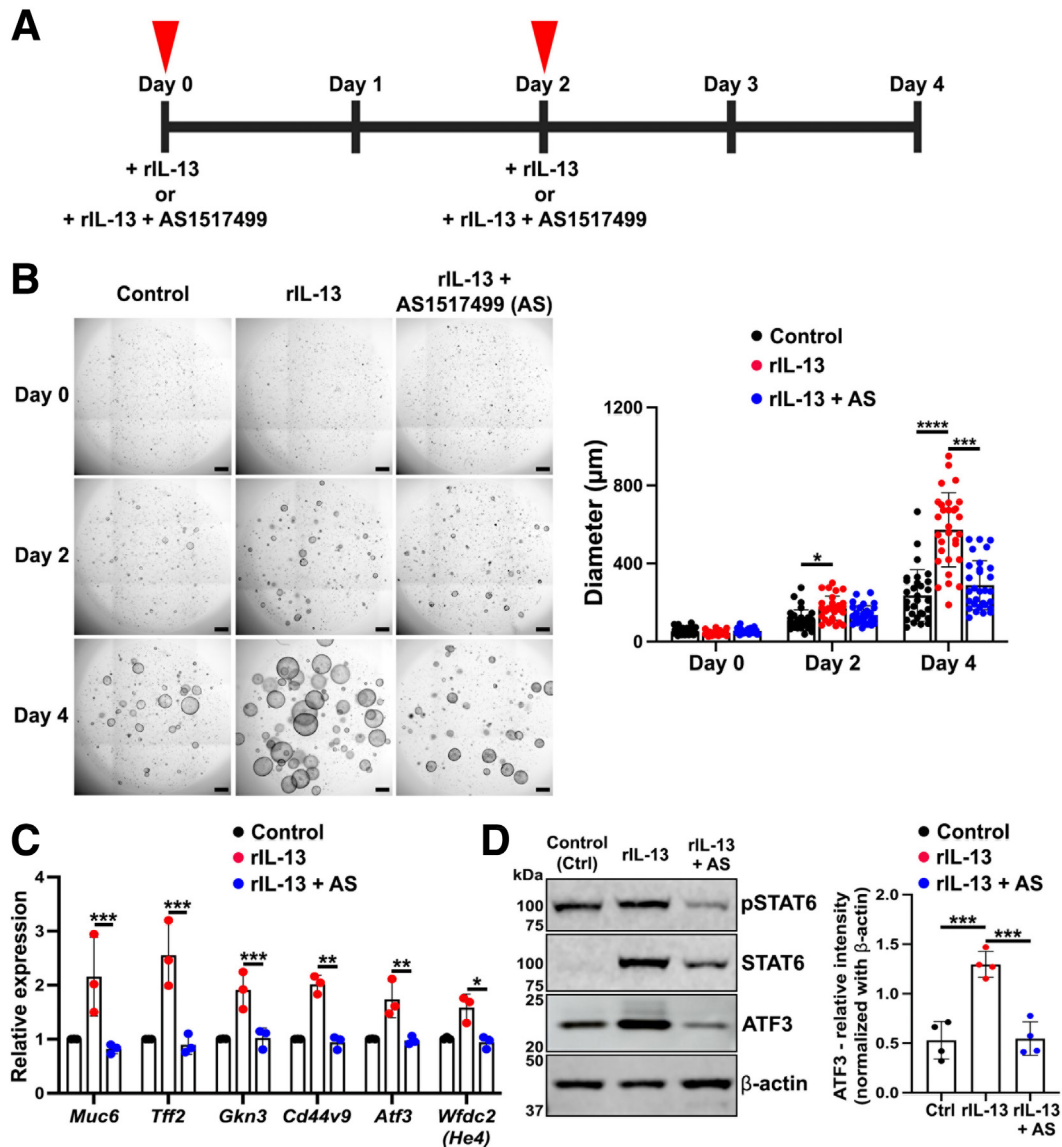


**Figure 12. AS1517499, a STAT6 inhibitor, impacted Meta1 gastroid growth and gene expression.** (A) Time-course diagram of the treatment to Meta1 gastroids with rIL-13 and/or AS1517499. (B) Representative bright field images of Matrigel domes containing Meta1 gastroids at different times of treatment. Quantitation of gastroid diameters showed a significant difference in Meta1 gastroids treated with AS1517499. Scale bar: 500  $\mu\text{m}$ . Mean  $\pm$  SD (N = 3 independent experiments). \* $P$  < .05, \*\*\* $P$  < .001, \*\*\*\* $P$  < .0001. (C) Quantitative RT-PCR showing relative expression levels of SPEM-related genes (*Muc6*, *Tff2*, *Gkn3*, *Cd44v9*, *Atf3*, and *He4*). Mean  $\pm$  SD (N = 3 independent experiments). \* $P$  < .05, \*\* $P$  < .01, \*\*\* $P$  < .001. (D) Immunoblotting shows significant down-regulation of phosphorylated STAT6 and ATF3 in Meta1 gastroids treated with STAT6 inhibitor (AS). Mean  $\pm$  SD (N = 4 independent experiments). \*\*\* $P$  < .001.

Pdx1, a lineage marker for pyloric glands. Previous studies have used primary corpus gastroids *in vitro*, and these do give rise to lineages with SPEM characteristics, but these cultures are often difficult to maintain past early passages. Thus, the availability of a continuously passaging Meta1 line with SPEM characteristics represents an important adjunct to primary gastroids as well as passaging human metaplastic gastroid lines. Furthermore, the Meta1 gastroids facilitate the study of mechanisms involved in the maturation and proliferation of SPEM cells, which would support regeneration of the stomach epithelial lining after damage. As in the case with many organoid preparations, Meta1

gastroids do not show full maturation in the Intesticult media used for their propagation. Still, addition of IL-13 promoted more complete maturation in both Meta1 gastroids as well as the human metaplastic gastroids with SPEM characteristics, with up-regulation of the expression of mucin-related proteins.

Recent studies have demonstrated that there is an accumulation of activated ILC2s, double positive for GATA3 and IL-13, in stomach mucosa of human and mouse samples with pyloric metaplasia.<sup>23,50,51</sup> Even though IL-25 and IL-33 can induce the accumulation and activation of ILC2s leading to their release of IL-13, our previous studies have shown



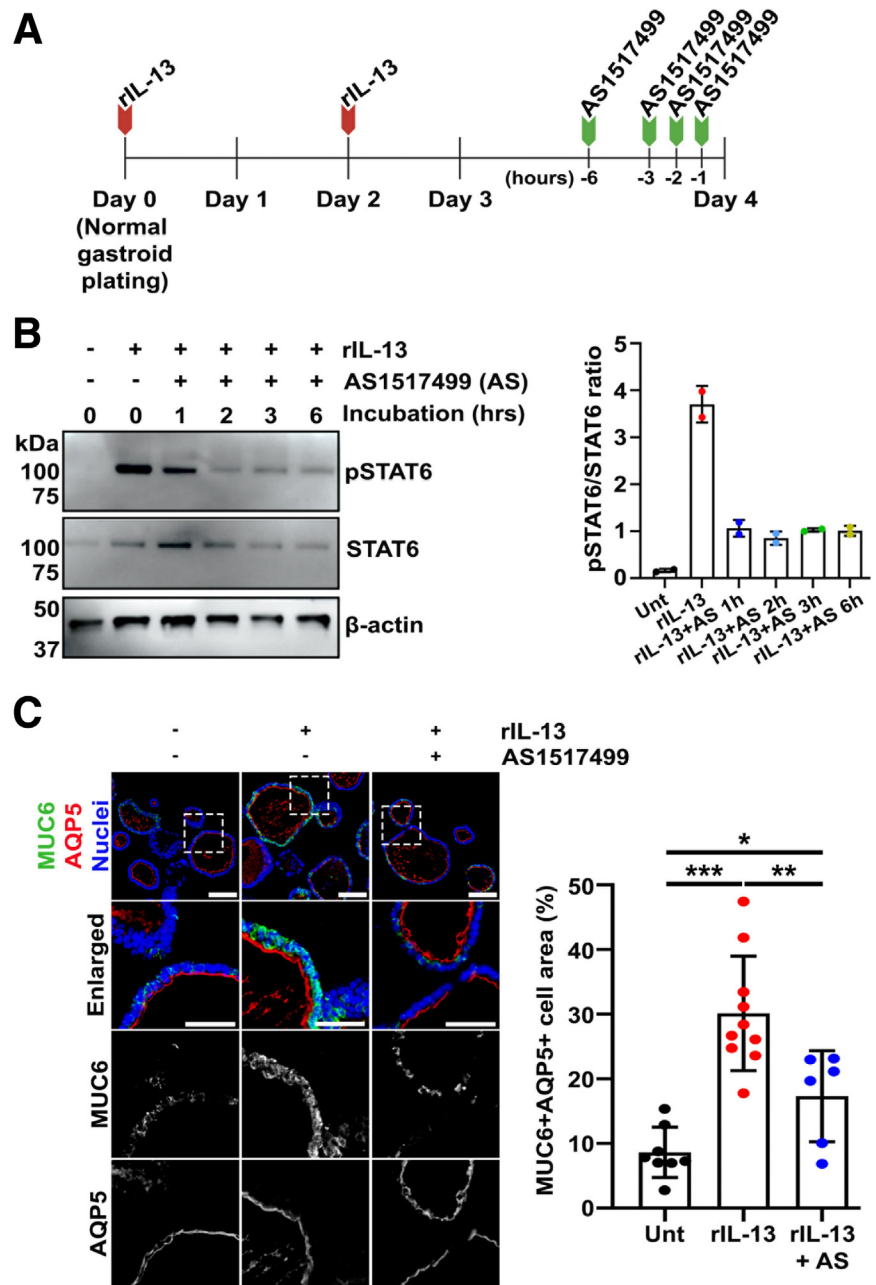


**Figure 13.** AS1517499 attenuated maturation of transdifferentiating cells into SPEM mucinous cells. (A) Time-course diagram of treatment of normal gastroids with rIL-13 and/or AS1517499 for immunoblotting experiments. (B) Immunoblotting shows down-regulation of phosphorylated STAT6 in normal gastroids treated with both rIL-13 and AS1517499. The phosphorylation decrease was evident beginning at 1 hour of AS1517499 addition. Quantitation showed that this decrease occurred in a time-dependent manner. Mean  $\pm$  SD (N = 2 independent experiments). (C) Immunofluorescence staining of normal gastroids cross sections treated with rIL-13 and/or AS1517499 for SPEM-related markers, MUC6 and AQP5. Quantitation of MUC6 and AQP5 double positive cells demonstrated significant decrease in proportion of mature SPEM cells as seen by reduction of MUC6 in the gastroids exposed to the STAT6 inhibitor. Scale bar: 100  $\mu$ m and 50  $\mu$ m for enlarged. Mean  $\pm$  SD (N = 4 independent experiments). \*P < .05, \*\*P < .01, \*\*\*P < .001.

that a cascade through IL-33 acting on ILC2s is key for the development of pyloric metaplasia and for potentially promoting mucosa repair.<sup>23,29</sup> In contrast, a recent study using different mouse models has suggested that the IL-25/ILC2s axis could promote the progression of metaplastic cells into neoplastic cells.<sup>50</sup> Activated ILC2s can also promote infiltration of other immune cells including macrophages and eosinophils.<sup>23</sup> These findings suggest that ILC2s can be a key producer of IL-13 and likely the first intramucosal immune cell response to severe damage in the gastric epithelium. In addition, recent studies have shown that ILCs could maintain their activated state *in vitro* co-culture systems with intestinal-type organoids.<sup>52,53</sup> In the present

studies, the 3D co-culture of activated ILC2s and Meta1 gastroids facilitated Meta1 gastroid exposure to the cytokines released by the ILC2s. This interaction promoted maturation of SPEM lineage cells with elevated expression of mucin-related proteins like TFF2 and MUC6. SPEM cell proliferation was also increased. Furthermore, we demonstrated that ILC2s co-cultured with Meta1 gastroids stimulated STAT6 phosphorylation in gastroid cells. This phosphorylation is likely stimulated by the cytokine IL-13 released by the ILC2s. Collectively, these data suggest that ILC2s remain activated and produce IL-13 *in vitro*, leading to the maturation and proliferation of SPEM cell lineages in the Meta1 gastroids.

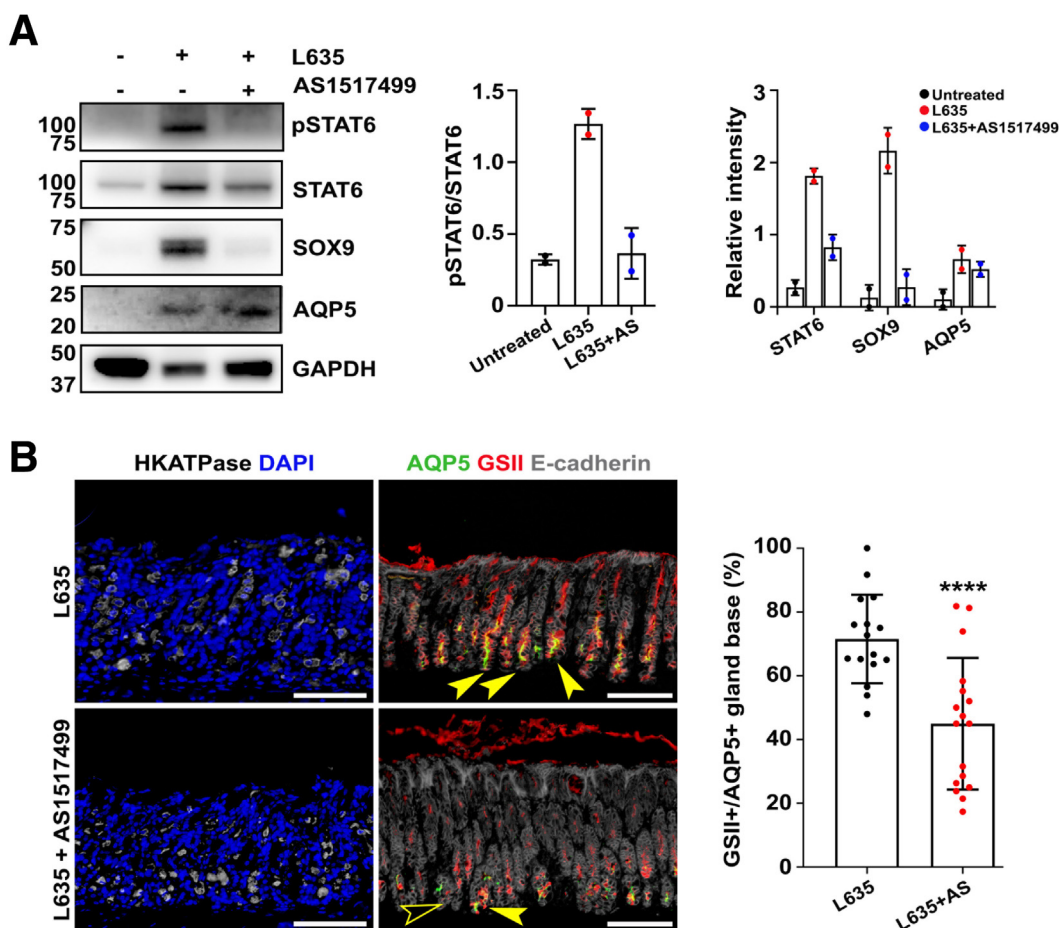


**Figure 14. AS1517499 attenuated development of SPEM in stomachs of mice treated with L635.** (A) Immunoblotting shows down-regulation of phosphorylated STAT6 and SOX9, a SPEM cell marker, in stomachs from mice treated with both L635 and AS1517499. Quantitation shows decreasing trend in STAT6 and SOX9 band intensity. Mean  $\pm$  SD (N = 2 independent experiments). (B) Immunofluorescence staining of stomach tissues for H-K-ATPase, a parietal cell marker, and SPEM cell markers including AQP5 and GSI1. Yellow arrowheads indicate GSI1<sup>+</sup>/AQP5 positive SPEM cells, while GSI1 or AQP5 negative cells are indicated by an empty arrowhead. Quantitation of average percentage of gland bases expressing both AQP5 and GSI1 markers showed significant decrease under L635 and AS1517499 combined treatment. Mean  $\pm$  SD (N = 16–17 images from 3 mice of each group). \*\*\*\**P* < .0001.

Previous investigations have suggested that IL-13 during inflammation plays a key role in metaplasia by increasing mucous cell hyperplasia in airway, intestinal, and other epithelial tissues.<sup>54–56</sup> In a previous study, we have demonstrated that acute induction of parietal cell loss leads to an expansion of ILC2 cells in the gastric mucosa and an increase in their expression of IL-13.<sup>23</sup> Moreover, IL-13, mainly derived from mast cells, can directly interact with stomach gastric epithelium in an autoimmune gastritis model and likely is responsible for induction of SPEM.<sup>34</sup> Although increases in mast cells have not been observed in the acute parietal cell loss models of SPEM, all of these studies support the concept that IL-13 is an important stimulator of SPEM induction. In the present study, we demonstrated that IL-13 derived from activated ILC2 cells, isolated from IL13-tdTomato mice after L635 treatment, can directly affect maturation of SPEM cells in the Meta1 gastroids *in vitro*. As observed with ILC2 co-culture, IL-13 treatment in Meta1 gastroids promoted SPEM cell

maturation by increasing expression of TFF2 and MUC6. SPEM cell proliferation was also increased. In addition, treatment with IL-13 triggered phosphorylation of STAT6 in a concentration-dependent manner. We also showed that gastroids generated from healthy normal mice demonstrated an increase in mature SPEM cells with dual expression of MUC6 and AQP5 after exposure to rIL-13 *in vitro*. Furthermore, human metaplastic gastroids treated with rIL-13 displayed similar increases in growth, pSTAT6, and SPEM cell maturation and proliferation as observed in Meta1 gastroids. Importantly, we have previously shown that this same human metaplastic gastroid line undergoes dysplastic transition when co-cultured with metaplasia-derived or cancer-derived fibroblasts.<sup>44</sup> Collectively, these data indicate that IL-13 can promote the maturation and proliferation of SPEM cells rather than progression toward dysplasia. Because pyloric metaplasia is initially a reparative lineage, IL-13 appears to support the maturation of SPEM cells with more mucin production and also

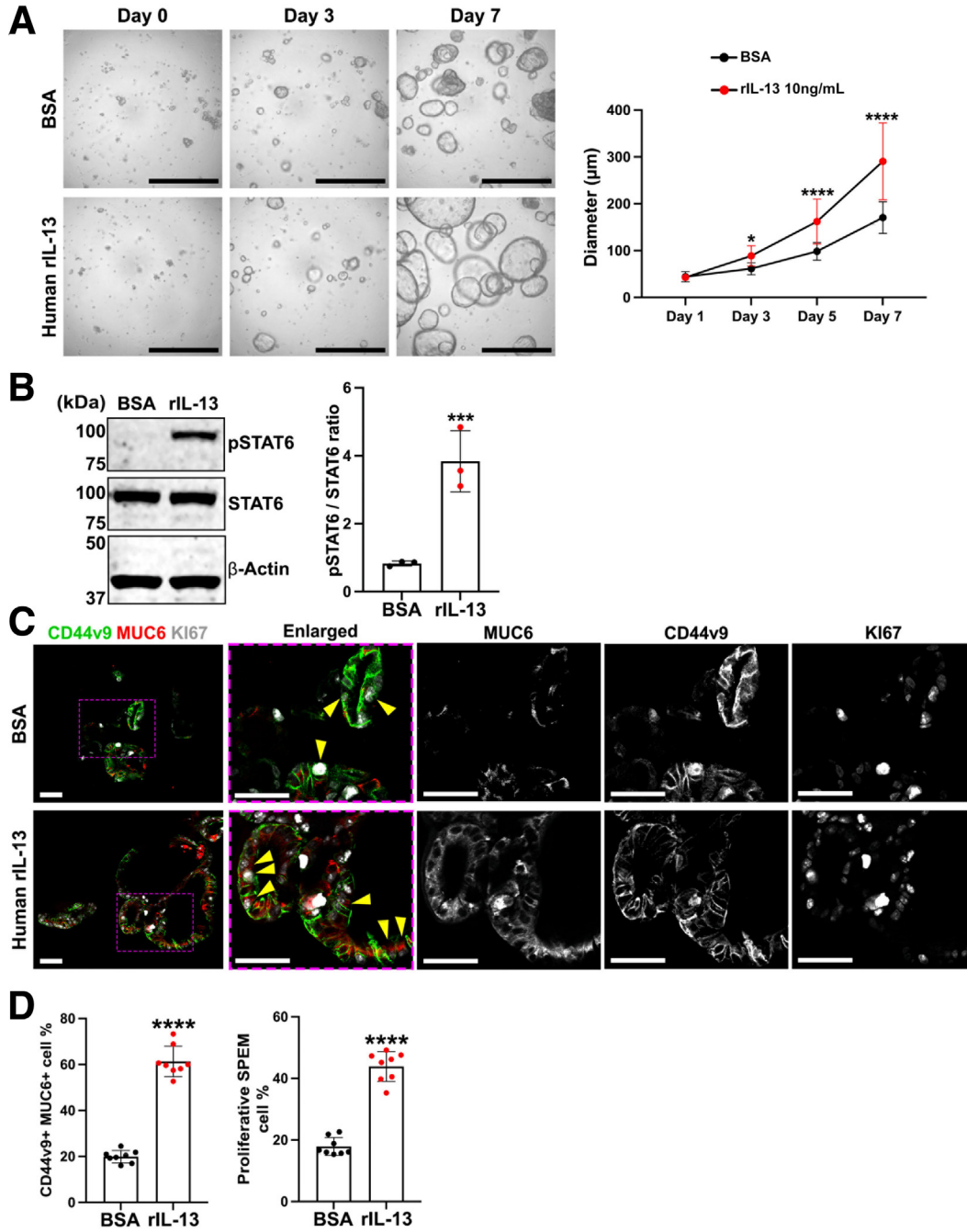


**Figure 15. Human rIL-13 promotes phosphorylation of STAT6 and maturation and proliferation in SPEM cells in human metaplastic gastroids.** (A) Representative bright field images of Matrigel domes containing human metaplastic gastroids treated with either rIL-13 or control (BSA). Quantitation of matched gastroid diameters showed significantly higher sizes in gastroids treated with rIL-13 compared with control after 5 days of treatment. Scale bar: 500  $\mu$ m for brightfield. Mean  $\pm$  SD (N = 3 independent experiments). \*\*\*\* $P$  < .0001. (B) Immunoblotting shows up-regulation of pSTAT6 in human metaplastic gastroids treated with rIL-13. Mean  $\pm$  SD (N = 3 independent experiments). \*\*\* $P$  < .001. (C) Immunofluorescence staining of human metaplastic gastroids cross sections for Ki67, a proliferation marker, and SPEM-related markers, MUC6 and CD44v9. Quantitation of MUC6 and CD44v9 double positive cells demonstrated significant increase in proportion of mature SPEM cells in rIL-13-treated gastroids. (D) Quantitation of MUC6, CD44v9, and Ki67 triple positive cells demonstrated significant increase in proportion of proliferative SPEM cells. Yellow arrowheads indicate triple positive mature and proliferative SPEM cells. Scale bar: 50  $\mu$ m. Mean  $\pm$  SD (N = 8 from 3 independent experiments). \*\*\*\* $P$  < .0001.

the proliferation of SPEM cells to repopulate the injured mucosa as part of the protective role of pyloric metaplasia.

Phosphorylated STAT6 can be an important regulator of gene transcription in airway epithelial cells<sup>57</sup>; however, its functionality in stomach epithelial cells remains unclear.



Phosphorylated STAT6 can translocate to the nucleus and bind to gene promoter regions to control transcription of diverse genes.<sup>41</sup> Here we demonstrated that in normal and Meta1 gastroids, IL-13 promoted STAT6 phosphorylation in concert with an increase of mature SPEM cells expressing mucin-like proteins including MUC6 and TFF2. Importantly, we have shown that SPEM-related genes, including *Muc6*, *Tff2*, *Gkn3*, *CD44v9*, *Atf3*, and *Wfdc2* (*He4*), contain putative STAT6-binding motifs within their promoter regions. We demonstrated that the IL-13/STAT6 axis promoted increase in gene transcription of these genes. In the same context, inhibition of STAT6 in normal gastroids, Meta1 gastroids, and mice prevented the increase of STAT6 phosphorylation, SPEM cell maturation, and SPEM-related gene transcription. The studies presented here indicate that the IL-13/STAT6 axis is key for the development, maturation, and proliferation of SPEM cells in different gastroid lines. Furthermore, our studies using AS1517499, a specific STAT6 inhibitor,<sup>43</sup> demonstrated that blocking of STAT6 inhibited the IL-13-dependent increase in SPEM cell maturation and proliferation. Together, these findings suggest that the IL-13/STAT6 axis promotes the production of mucinous proteins and proliferation resulting in a mature and proliferative SPEM cell phenotype.

The transdifferentiation process of chief cells toward SPEM cells after gastric damage is a well-orchestrated process with the involvement of different master transcription factors. Recent studies have shown that activating transcription factor 3 (ATF3) is a key regulator in the early stages of the chief cell transdifferentiation process into SPEM cells.<sup>58</sup> ATF3 can repress Mist1, a transcription factor in charge of chief cell maturation, and activate pathways for proper clearance of specialized chief cell granules. Moreover, ATF3 could also regulate transcriptional pathways related to cell survival and proliferation to ensure that metaplastic/SPEM cells can fully protect the gastric epithelium after injury. To our knowledge, it is not known how ATF3 is up-regulated after gastric injury. This study demonstrated that IL-13-treated Meta1 gastroids display up-regulation of ATF3 mRNA and protein and that the *Atf3* gene contains STAT6-binding promoter regions. These observations suggest that STAT6 may up-regulate ATF3 early after gastric injury after activation of ILC2s and release IL-13.

Pyloric metaplasia is generally thought to emerge after a well-coordinated intrinsic immune response to repair and/or resolve gastric injury in the stomach mucosa.<sup>59</sup> Although many studies have supported a role for inflammation as a promoter of carcinogenesis, IL-13 does not appear to promote carcinogenic transitions in SPEM cells in the present studies. Meta1 and human metaplastic gastroids treated with IL-13 alone did not promote progression of SPEM cells into dysplastic lineages but rather promoted a mature and mucinous SPEM cell phenotype. Although the dysplastic potential of Meta1 gastroids is unclear at this time, because the human gastric line used in these studies can undergo dysplastic transitions when co-cultured with metaplasia and dysplasia-derived fibroblasts, the present studies indicate that SPEM lineages can be influenced toward both metaplastic and dysplastic fates. Therefore, here we suggest the concept that IL-13-driven activation of STAT6 pathway

promotes the development, maturation, and proliferation of SPEM cells<sup>23</sup> as a protective mucinous metaplasia. This pattern of SPEM maturation would promote mucosal protection until gastric damage is resolved and allow return of normal gastric lineages. The actions of IL-13 released from intrinsic mucosal ILC2s or other immune cell populations may represent an important mucosal gatekeeper function for promotion of non-neoplastic protection of the gastric mucosa.

## Materials and Methods

### Mouse Models

Using the previously established mouse model, Mist1-CreERT2<sup>Tg/+</sup>; LSL-Kras (G12D)<sup>Tg/+</sup>; Rosa26-mTmG (Mist1-Kras-mTmG),<sup>9</sup> we induced Kras activation in chief cells to develop pyloric metaplasia. Briefly, female or male mice were given a total of 5 mg of tamoxifen dissolved in corn oil and 10% ethanol for 3 consecutive days by subcutaneous injection. Mice were killed at 1 month after the tamoxifen injections, and the stomachs were collected. The IL-13-tdTomato mice were generated as previously described,<sup>39</sup> and we received them as a gift from Dr Andrew N. J McKenzie, Cambridge, UK. The care, maintenance, and treatment of the mice used in this study followed protocols approved by the Institutional Animal Care and Use Committee of Vanderbilt University.

### Mouse and Human Gastroid Generation

Human metaplastic gastroids were established and characterized previously.<sup>44</sup> Meta1 gastroid lines were generated as previously described.<sup>37</sup> In brief, the Mist1-Kras-mTmG mouse stomachs were collected after 1 month of tamoxifen induction, and corpus mucosa was isolated. The corpus mucosa was then digested to obtain individual glands using collagenase. After that, digested solutions were quenched and strained in 100- $\mu$ m cell strainer to remove remaining tissue clumps. The isolated glands were washed, pelleted, and then resuspended with Matrigel (ECM, Sigma-Aldrich). We added 30  $\mu$ L of Gland/Matrigel mix per well in a 48-well-plate. Three hundred  $\mu$ L of Mouse IntestiCult (StemCell Technology) medium with a ROCK inhibitor (Y-27632) was added in each well, and medium was replaced every 3 days. Wild-type mouse stomachs were harvested for the establishment of normal gastroids following the same protocol for Meta1 gastroid generation.

### Single-Cell RNA Sequencing Analysis

The scRNA-seq was performed using single cell encapsulation technology as reported previously.<sup>37,60</sup> Briefly, for each gastroid line, a total of 7–8 Matrigel domes containing gastroids were pooled together to generate single-cell suspension. Dead cells were removed using the EasySep Dead Cell Removal (Annexin V) kit (StemCell Technologies) before encapsulation. Live single cells were encapsulated and barcoded according to inDrop (1CellBio) platform recommendations. Sequencing libraries were prepared following the TruDrop library preparation protocol.<sup>61</sup> After library preparation and sequencing, reads were filtered and

processed to obtain high-quality cells using the inDrop pipeline, as reported previously.<sup>37</sup> This resulted in a pre-processed data matrix containing approximately 5000–7000 single cells per gastroid line. The pre-processed data matrices containing gene expression profiles were uploaded to the Partek Flow suite for their further analysis. After cell and feature filtering and normalization in Partek, we obtained high quality cells for each gastroid line. The cells from the 3 samples were clustered using graph-based clustering on the informative principal component analysis space ( $n = 10$ ). We used UMAP for data visualization. The 3 main clusters of cells found were annotated by the expression of known marker genes of SPEM and dysplastic cells. Finally, differential expression analysis was performed on samples (Meta1 and Meta4 gastroids) and on clusters within Meta1 gastroids (Meta1-A, Meta1-B).

### Activated ILC2s Isolation and Cell Sorting/Flow Cytometry

The ILC2s isolation was performed as previously described.<sup>23</sup> IL-13-tdTomato mice were given L635 compound (synthesized by Vanderbilt Institute of Chemical Biology), dissolved in phosphate-buffered saline (PBS), by oral gavage at a concentration of 350 mg/kg once a day for 3 consecutive days. At day 3, the mouse stomachs were harvested, and corpus mucosa was isolated. Corpus mucosa was finely chopped with a razor blade and resuspended in ice cold Advanced Dulbecco modified Eagle medium (DMEM)/F12 cell culture medium. After the minced tissue settled, supernatant was removed leaving behind few milliliters of medium with gastric mucosa. Stomach corpus pieces were chemically digested with 1 U/mL of dispase in DMEM/F-12 (Corning) for 7 minutes at 37°C and then passed through a 100- $\mu$ m filter (Corning) and crushed with a rubber syringe plunger into a single-cell suspension over a 15-mL conical tube. Cells were centrifuged twice at 500g for 10 minutes at 4°C and resuspended in PBS with 3% fetal bovine serum to remove excess cell debris and media. Before cell sorting, cells were washed twice in PBS with 3% fetal bovine serum and incubated with 40,6-diamidino-2-phenylindol (DAPI). IL-13 positive cells were sorted using the 5-Laser FACS Aria III from the VUMC Flow Cytometry Shared Resources. On the machine, samples were initially segregated from debris using forward scatter and side scatter properties of the 555-nm laser. Dead cells were excluded on the basis of their DAPI staining. Endogenous tdTomato+ cells were sorted directly into DMEM/F-12 with 10% fetal bovine serum using a 100- $\mu$ m nozzle.

### ILC2s and Meta1 Gastroid 3D Co-culture

Sorted active ILC2s were co-cultures with Meta1 gastroids in Matrigel. Ready to split Meta1 gastroids were minced into small pieces and resuspended in 15  $\mu$ L of Matrigel, and they were mixed with a total of 2500 sorted IL-13-positive ILC2s resuspended in 15  $\mu$ L of Matrigel. The final 30  $\mu$ L was well-mixed and plated in a 48-well plate in dome shape. The plate was incubated at 37°C for 30 minutes to let the Matrigel solidify. After that, we added 300  $\mu$ L of IntestiCult medium (StemCell Technologies) including

rIL-2, 25 (rIL-25), and 33 (rIL-33), and medium was changed every other day up to 5 days.

### Human Metaplastic, Meta1, and Normal Gastroids Treatment With Recombinant IL-13, IL-4, and STAT6 Inhibitor

Ready to split gastroids were collected, minced into small pieces, resuspended in 30  $\mu$ L of Matrigel, and plated in a dome shape in a 48-well plate. The plate was incubated at 37°C for 30 minutes to let the Matrigel solidify. After that, we added 300  $\mu$ L of IntestiCult medium and returned the plate to the incubator. Plates were left to rest for 24 hours in the incubator before the start of treatment to allow the small pieces of gastroids to form sphere-like structures. IntestiCult medium was combined with either 0.1% BSA (control/vehicle) or rIL-13/rIL-4. For Meta1 gastroids, rIL-13 or rIL-4 was used at a 1 ng/mL concentration. For human metaplastic gastroids, rIL-13 was used at a 10 ng/mL concentration. For normal gastroids, we used 1, 3, and 10 ng/mL of rIL-13. Three hundred  $\mu$ L of control or rIL-13/rIL-4 medium was replaced in the gastroids plated 24 hours before. Medium was replaced every other day. For STAT6 inhibition studies, 1  $\mu$ mol/L AS1517499 was added together with rIL-13 accordingly. At the end of treatments, gastroids were collected and processed for further analysis.

### Air-Liquid Interface Culture

We performed the ALI culture as previously described.<sup>44</sup> Briefly, Meta1 gastroids were treated with Organoid Harvesting Solution (Cultrex) for Matrigel removal following manufacturer's instructions. Gastroids were centrifuged and resuspended in IntestiCult medium with ROCK inhibitor. Gastroids were minced into small pieces containing around 10–20 cells in each piece. The small pieces were centrifuged and resuspended again with corresponding medium (rIL-13 or BSA). Transwell filters were previously coated with type I collagen (2.7 mg/cm<sup>2</sup>). A total of 400  $\mu$ L of medium was added to the well below the filter, and a total of 200  $\mu$ L of medium containing minced Meta1 gastroids was added on top of the filter. Medium was replaced every other day. After 7 days, Meta1 gastroids cells covered the entire surface of the filter, and medium on the top was removed to start the ALI culture. Medium below the filter was changed and mucin secretions on top of the filter were removed every other day. Meta1 gastroid cells were in ALI for 4 weeks.

### Whole Mount Staining of Transwell Filters

Whole mount staining was performed as reported previously.<sup>62</sup> In brief, Transwell filters containing Meta1 gastroid cells were washed with PBS 3 times and then fixed in 4% paraformaldehyde. Transwells were blocked with 0.3% Triton X-100 and 10% NDS in PBS for 60 minutes at room temperature. Primary antibodies in PBS containing 0.1% Tween 20 (PBST) and 1% NDS were applied overnight at 4°C. The filters were washed with PBST 3 times and then incubated with secondary antibodies in PBST with 1% NDS for 1 hour at room temperature. Counterstaining was

performed using Hoechst in PBS (1:5000) at room temperature for 5 minutes. Transwell filters were cut from plastic insert and mounted in a slide using ProLong Gold Antifade mounting media (Thermo Fisher) and a cover slide.

### Human Metaplastic Gastroid High-Throughput Culture

We used the ASFA SPOTTER V6 (MBD, Gyeonggi-do, Republic of Korea),<sup>61</sup> an automated dispenser, to seed and grow human metaplastic gastroids in 384-pillar plates. We seeded a total of 2  $\mu$ L of Matrigel (ECM, Corning) containing gastroid pieces of around 10–20  $\mu$ m onto each pillar, with a total of 30–40 pillars per condition. We let the Matrigel solidify at 37°C for 1 hour and inverted the pillars into 40  $\mu$ L of Human IntestiCult medium supplemented with either BSA control or rIL-13. We changed the medium every other day for up to a week. The human gastroids were fixed, removed from the pillars, and processed into OCT for frozen sectioning and immunostaining.

### Quantitative Real-Time PCR Analysis

Meta1 gastroids were collected, and Matrigel was removed with Organoid Harvesting Solution following manufacturer's instructions. Total RNA was isolated using Trizol (Invitrogen) reagent. The DNase I Amplification Grade kit (Thermo Fisher) was used for removal of any DNA leftover, and the iScript gDNA Clear cDNA Synthesis Kit (Thermo Fisher) was used for complementary DNA synthesis. Quantitative RT-PCR was performed using pair of specific primers for targeted genes (Table 1) and using the SsoAdvanced Universal SYBR Green Super Mix (Bio-Rad) on the Bio-Rad CFX96 Touch Real-Time PCR Detection System; the raw data were analyzed using the CFX Maestro software (Bio-Rad). The TBP gene expression was used for normalization of mRNA transcripts, and it is shown as relative expression levels.

### STAT6 Inhibitor Treatment to Wild-Type Mice

Wild-type mice were administered with L635 (synthesized by the Vanderbilt Institute of Chemical Biology) dissolved in PBS by oral gavage at a concentration of 350 mg/kg once a day for 3 consecutive days without or with 5 mg/kg of AS1517499, a STAT6 inhibitor (Selleckchem). After 3 days of treatment, stomachs were harvested for further analysis.

### Immunoblotting

Treated or untreated gastroids were collected, and Matrigel was removed with Organoid Harvesting Solution following manufacturer's instructions. Total protein was isolated using M-PER lysis buffer (Thermo Fisher Scientific) with protease and phosphatase inhibitor cocktails. Protein concentration measurements were performed using the Direct Detect IR spectrometer (Millipore). For protein separation, a total of 20  $\mu$ g was loaded in NuPAGE 10% BisTris Precast Gel (Invitrogen). The separate proteins were transferred to a nitrocellulose membrane (Bio-Rad). For

**Table 1.** Quantitative qPCR Primer Sequences

#### Oligonucleotides

##### *mCD44v9 primers*

F: 5' GGAGATCAGGATGACTCCTTCT 3'

R: 5' AGTCCTGGATGAGTCTCGATC 3'

##### *mMuc6 primers*

F: 5' GGAAC TAACAGTCTGGACCACC 3'

R: 5' CTTCGGTATGGATGTAGGAGGC 3'

##### *mTff2 primers*

F: 5' TGCTTTGATCTTGGATGCTG 3'

R: 5' GGAAAAGCAGCAGTTTCGAC 3'

##### *mGkn3 primers*

F: 5' CCTTATCATAGTGAGACCTGAG 3'

R: 5' CAATAAGGCGTCTCATGTTG 3'

##### *mClu primers*

F: 5' CCAGCCTTTCTTTGAGATGA 3'

R: 5' CTCCTGGCACTTTTCACACT 3'

##### *mAQP5 primers*

F: 5' CGCTCAGCAACAACAACACC 3'

R: 5' GACCGACAAGCCAATGGATAAG 3'

##### *mGif primers*

F: 5' CCCTCTACCTCCTAAGTGTCTC 3'

R: 5' CTGAGTCAGTCACCGAGTTCT 3'

##### *mHe4 primers*

F: 5' TGCTGCCTGTGCGCTCTG 3'

R: 5' TGTCCGCACAGTCCTTGCCA 3'

##### *mTbp primers*

F: 5' CAAACCCAGAATTGTTCTCCTT 3'

R: 5' ATGTGGTCTTCTGAATCCCT 3'

F, forward; R, reverse.

protein detection we used 2 systems, the Odyssey imaging system (LI-COR Biociences) and the Amersham Imager 680 instrument (GE Healthcare), and followed the manufacturer's instructions. Membranes were blocked with 5% BSA, skim milk, or Odyssey blocking solution depending on the primary antibody of interest. Used primary and secondary antibodies are listed in Table 2. GAPDH or  $\beta$ -actin was used as a loading control. SuperSignal West Femto Maximum Sensitivity Substrate (Thermo Fisher) was applied to the membranes for the Amersham Imager 680.

### Immunofluorescence Staining of Paraffin-Embedded Tissue or Gastroid Sections

For processing of gastroids or mouse tissue we followed standard procedures previously reported.<sup>17,23,37</sup> Mouse stomach tissues were fixed with 4% paraformaldehyde overnight, processed, and then embedded on paraffin. Briefly for gastroid embedding, Matrigel domes containing gastroids were fixed with 4% paraformaldehyde at room temperature for 20 minutes with gentle rocking, followed by a wash in PBS at room temperature for 5 minutes. The fixed Matrigel domes were preserved in the HistoGel (Thermo



**Table 2.** Antibodies Used

Antibody	Species	Source	Dilution
CD44v9	Rat	Cosmo Bio, LKG-M002	1:25,000
AQP5	Rabbit	Sigma-Aldrich, HPA065008	1:500
TROP2	Goat	R&D Systems, AF1122	1:500
TFF2	Mouse	Abcam, ab203237	1:500
MUC6	Mouse	Abcam, ab216017	1:200
Ki67	Rat	Biologend, 652402	1:200
GSII lectin, Alexa Fluor 647 conjugated		Molecular probes, L32451	1:2000
STAT6	Rabbit	Cell Signaling Technology, 5397S	1:1000
pSTAT6	Rabbit	Cell Signaling Technology, 56554S	1:1000
ATF3	Rabbit	Novus, NBP1-85816	1:500
$\beta$ -Actin	Mouse	Sigma-Aldrich, A5316	1:5000

Fisher Scientific) and then processed for paraffin embedding handled by the Translational Pathology Shared Resource from Vanderbilt University Medical Center. Slides containing 5  $\mu$ m formalin-fixed paraffin embedded sections were deparaffinized in HistoClear solution (Electron Microscopy Services) and rehydrated in a series of ethanol washes (100%, 95%, 70%). Using a target retrieval solution of pH 6 from Dako, antigen retrieval was performed in a pressure cooker for 15 minutes. Sections were incubated in Serum-free Protein Block solution (Dako) at room temperature for 90 minutes. Primary antibodies were diluted in Antibody Diluent with background reducing components (Dako) and applied for overnight incubation at 4°C. Next day after 3 washes with PBS, secondary antibodies diluted in Antibody Diluent were applied to sections and incubated at room temperature for 60 minutes, followed by another 3 washes in PBS. Used primary antibodies are listed in Table 2. Nuclei counterstaining was performed by section incubation with either DAPI or Hoechst in PBS (1:5000) at room temperature for 5 minutes. This was followed by 3 washes with PBS and slide mounting using ProLong Gold Antifade Mountant (Thermo Fisher) and a cover slide. Immunofluorescence images were acquired using a Zeiss Axio Imager M2 using a 20 $\times$  objective. Image overlay and preparation were performed in Adobe Photoshop.

### Statistical Analysis

All authors had access to the study data and had reviewed and approved the final manuscript. Data are expressed as dot plots showing mean  $\pm$  standard deviation (SD). Differences were analyzed by Student unpaired *t* test (two-tailed) when 2 groups were analyzed and by one-way analysis of variance (two-tailed) when more than 2 groups were analyzed. Tukey's multiple comparison post hoc test was used with one-way and two-way analysis of variance.  $P < .05$  was considered significant. All statistical analyses were performed with GraphPad Prism (version 10.0.2; 2023 GraphPad Software, LLC).

### References

1. Siegel RL, Miller KD, Wagle NS, et al. Cancer statistics, 2023. *CA Cancer J Clin* 2023;73:17–48.
2. Sung H, Ferlay J, Siegel RL, Laversanne M, et al. Global cancer statistics 2020: GLOBOCAN estimates of incidence and mortality worldwide for 36 cancers in 185 countries. *CA Cancer J Clin* 2021;71:209–249.
3. Morgan E, Arnold M, Camargo MC, et al. The current and future incidence and mortality of gastric cancer in 185 countries, 2020–40: a population-based modelling study. *EClinicalMedicine* 2022;47:101404.
4. Correa P. A human model of gastric carcinogenesis. *Cancer Res* 1988;48:3554–3560.
5. Lynch P. Biology of gastric cancer: gastritis-metaplasia-dysplasia sequence, role of *H. Pylori*, and molecular correlates of tumor progression. *J Infus Chemother* 1995;5:93–96.
6. Mills JC, Goldenring JR. Metaplasia in the stomach arises from gastric chief cells. *Cell Mol Gastroenterol Hepatol* 2017;4:85–88.
7. Nomura S, Baxter S, Yamaguchi T, et al. Spasmolytic polypeptide expressing metaplasia (SPEM) to preneoplasia in *H. felis*-infected mice. *Gastroenterology* 2004;127:582–594.
8. Xia HH, Yang Y, Lam SK, et al. Aberrant epithelial expression of trefoil family factor 2 and mucin 6 in *Helicobacter pylori* infected gastric antrum, incisura, and body and its association with antralisation. *J Clin Pathol* 2004;57:861–866.
9. Choi E, Hendley AM, Bailey JM, et al. Expression of activated Ras in gastric chief cells of mice leads to the full spectrum of metaplastic lineage transitions. *Gastroenterology* 2016;150:918–930.
10. Schmidt PH, Lee JR, Joshi V, et al. Identification of a metaplastic cell lineage associated with human gastric adenocarcinoma. *Lab Invest* 1999;79:639–646.
11. Wong W-M, Garcia SB, Poulsom R, et al. Aberrant spasmolytic polypeptide (TFF2)-expressing cell lineage (SPEM), pseudopyloric metaplasia (PPM) and the response to gastric mucosal damage. *Gastroenterology* 1999;116:A525.
12. Bredemeyer AJ, Geahlen JH, Weis VG, et al. The gastric epithelial progenitor cell niche and differentiation of the zymogenic (chief) cell lineage. *Dev Biol* 2009;325:211–224.

13. Radyk MD, Burclaff J, Willet SG, et al. Metaplastic cells in the stomach arise, independently of stem cells, via dedifferentiation or transdifferentiation of chief cells. *Gastroenterology* 2018;154:839–843.e2.
14. Caldwell B, Meyer AR, Weis JA, et al. Chief cell plasticity is the origin of metaplasia following acute injury in the stomach mucosa. *Gut* 2021.
15. Nomura S, Baxter T, Yamaguchi H, et al. Spasmolytic polypeptide expressing metaplasia to preneoplasia in *H. felis*-infected mice. *Gastroenterology* 2004;127:582–594.
16. Brown JW, Cho CJ, Mills JC. Paligenosis: cellular remodeling during tissue repair. *Annu Rev Physiol* 2022; 84:461–483.
17. Lee S, Jang B, Min J, et al. Upregulation of AQP5 defines spasmolytic polypeptide-expressing metaplasia (SPEM) and progression to incomplete intestinal metaplasia. *Cell Molec Gastroenterol Hepatol* 2022; 13:199–217.
18. Goldenring JR, Mills JC. Cellular plasticity, reprogramming, and regeneration: metaplasia in the stomach and beyond. *Gastroenterology* 2022;162:415–430.
19. Willet SG, Lewis MA, Miao ZF, et al. Regenerative proliferation of differentiated cells by mTORC1-dependent paligenosis. *EMBO J* 2018;37.
20. Petersen CP, Weis VG, Nam KT, et al. Macrophages promote progression of spasmolytic polypeptide-expressing metaplasia following acute loss of parietal cells. *Gastroenterology* 2014;146:1727–1738.
21. Busada JT, Ramamoorthy S, Cain DW, et al. Endogenous glucocorticoids prevent gastric metaplasia by suppressing spontaneous inflammation. *J Clin Invest* 2019;129:1345–1358.
22. De Salvo C, Pastorelli L, Petersen CP, et al. Interleukin 33 triggers early eosinophil-dependent events leading to metaplasia in a chronic model of gastritis-prone mice. *Gastroenterology* 2021;160:302–316 e7.
23. Meyer AR, Engevik AC, Madorsky T, et al. Group 2 innate lymphoid cells coordinate damage response in the stomach. *Gastroenterology* 2020;159:2077–2091.e8.
24. Spits H, Di Santo JP. The expanding family of innate lymphoid cells: regulators and effectors of immunity and tissue remodeling. *Nat Immunol* 2011;12:21–27.
25. Eberl G, Colonna M, Di Santo JP, et al. Innate lymphoid cells: a new paradigm in immunology. *Science* 2015;348: aaa6566.
26. Stier MT, Bloodworth MH, Toki S, et al. Respiratory syncytial virus infection activates IL-13-producing group 2 innate lymphoid cells through thymic stromal lymphopoietin. *J Allergy Clin Immunol* 2016;138:814–824.e11.
27. Li D, Guabiraba R, Besnard AG, et al. IL-33 promotes ST2-dependent lung fibrosis by the induction of alternatively activated macrophages and innate lymphoid cells in mice. *J Allergy Clin Immunol* 2014; 134:1422–1432.e11.
28. Bernink JH, Germar K, Spits H. The role of ILC2 in pathology of type 2 inflammatory diseases. *Curr Opin Immunol* 2014;31:115–120.
29. Petersen CP, Meyer AR, De Salvo C, et al. A signalling cascade of IL-33 to IL-13 regulates metaplasia in the mouse stomach. *Gut* 2018;67:805–817.
30. McCormick SM, Heller NM. Commentary: IL-4 and IL-13 receptors and signaling. *Cytokine* 2015;75:38–50.
31. Hu X, Li J, Fu M, et al. The JAK/STAT signaling pathway: from bench to clinic. *Signal Transduct Target Ther* 2021; 6:402.
32. Li J, Rodriguez JP, Niu F, et al. Structural basis for DNA recognition by STAT6. *Proc Natl Acad Sci U S A* 2016; 113:13015–13020.
33. Karpathiou G, Papoudou-Bai A, Ferrand E, et al. STAT6: a review of a signaling pathway implicated in various diseases with a special emphasis in its usefulness in pathology. *Pathol Res Pract* 2021;223:153477.
34. Noto CN, Hoft SG, Bockerstett KA, et al. IL-13 acts directly on gastric epithelial cells to promote metaplasia development during chronic gastritis. *Cell Mol Gastroenterol Hepatol* 2022;13:623–642.
35. Sato T, Vries RG, Snippert HJ, et al. Single Lgr5 stem cells build crypt-villus structures in vitro without a mesenchymal niche. *Nature* 2009;459:262–265.
36. Jiang X, Oyang L, Peng Q, et al. Organoids: opportunities and challenges of cancer therapy. *Front Cell Dev Biol* 2023;11:1232528.
37. Min J, Vega PN, Engevik AC, et al. Heterogeneity and dynamics of active Kras-induced dysplastic lineages from mouse corpus stomach. *Nature Communications* 2019;10:5549.
38. Chung WC, Jung SH, Lee KM, et al. The detection of *Helicobacter pylori* cag pathogenicity islands (PAIs) and expression of matrix metalloproteinase-7 (MMP-7) in gastric epithelial dysplasia and intramucosal cancer. *Gastric Cancer* 2010;13:162–169.
39. Barlow JL, Bellosi A, Hardman CS, et al. Innate IL-13-producing nuocytes arise during allergic lung inflammation and contribute to airways hyperreactivity. *J Allergy Clin Immunol* 2012;129:191–198, e1–e4.
40. Nam KT, Lee H-J, Sousa JF, et al. Mature chief cells are cryptic progenitors for metaplasia in the stomach. *Gastroenterology* 2010;139:2028–2037.
41. Gour N, Wills-Karp M. IL-4 and IL-13 signaling in allergic airway disease. *Cytokine* 2015;75:68–78.
42. Castro-Mondragon JA, Riudavets-Puig R, Rauluseviciute I, et al. JASPAR 2022: the 9th release of the open-access database of transcription factor binding profiles. *Nucleic Acids Res* 2022;50:D165–D173.
43. Chiba Y, Todoroki M, Nishida Y, et al. A novel STAT6 inhibitor AS1517499 ameliorates antigen-induced bronchial hypercontractility in mice. *Am J Respir Cell Mol Biol* 2009;41:516–524.
44. Lee SH, Contreras Panta EW, Gibbs D, et al. Apposition of fibroblasts with metaplastic gastric cells promotes dysplastic transition. *Gastroenterology* 2023;165:374–390.
45. Weng G, Tao J, Liu Y, et al. Organoid: bridging the gap between basic research and clinical practice. *Cancer Lett* 2023;216353.
46. Chen Q, Weng K, Lin M, et al. SOX9 modulates the transformation of gastric stem cells through biased symmetric cell division. *Gastroenterology* 2023; 164:1119–1136.e12.
47. Fischer AS, Mullerke S, Arnold A, et al. R-spondin/YAP axis promotes gastric oxyntic gland regeneration and

- Helicobacter pylori-associated metaplasia in mice. *J Clin Invest* 2022;132.
48. Sue S, Shibata W, Kameta E, et al. Intestine-specific homeobox (ISX) induces intestinal metaplasia and cell proliferation to contribute to gastric carcinogenesis. *J Gastroenterol* 2016;51:949–960.
  49. Lo YH, Kolahi KS, Du Y, et al. A CRISPR/Cas9-engineered ARID1A-deficient human gastric cancer organoid model reveals essential and nonessential modes of oncogenic transformation. *Cancer Discov* 2021;11:1562–1581.
  50. O’Keefe RN, Carli ALE, Baloyan D, et al. A tuft cell - ILC2 signaling circuit provides therapeutic targets to inhibit gastric metaplasia and tumor development. *Nature Communications* 2023;14:6872.
  51. Zeis P, Lian M, Fan X, et al. In situ maturation and tissue adaptation of type 2 innate lymphoid cell progenitors. *Immunity* 2020;53:775–792.e9.
  52. Jowett GM, Read E, Roberts LB, et al. Organoids capture tissue-specific innate lymphoid cell development in mice and humans. *Cell Rep* 2022;40:111281.
  53. Moller KJ, Wegner LHM, Malsy J, et al. Expanded ILC2s in human infant intestines promote tissue growth. *Mucosal Immunol* 2023;16:408–421.
  54. Park KS, Korfhagen TR, Bruno MD, et al. SPDEF regulates goblet cell hyperplasia in the airway epithelium. *J Clin Invest* 2007;117:978–988.
  55. Horsnell WG, Cutler AJ, Hoving JC, et al. Delayed goblet cell hyperplasia, acetylcholine receptor expression, and worm expulsion in SMC-specific IL-4R $\alpha$ -deficient mice. *PLoS Pathog* 2007;3:e1.
  56. Tukler Henriksson J, Coursey TG, Corry DB, et al. IL-13 stimulates proliferation and expression of mucin and immunomodulatory genes in cultured conjunctival goblet cells. *Invest Ophthalmol Vis Sci* 2015;56:4186–4197.
  57. Kuperman DA, Huang X, Koth LL, et al. Direct effects of interleukin-13 on epithelial cells cause airway hyperactivity and mucus overproduction in asthma. *Nat Med* 2002;8:885–889.
  58. Radyk MD, Spatz LB, Peña BL, et al. ATF3 induces RAB7 to govern autodegradation in paligenosis, a conserved cell plasticity program. *EMBO Reports* 2021.
  59. Goldenring JR. Pyloric metaplasia, pseudopyloric metaplasia, ulcer-associated cell lineage and spasmolytic polypeptide-expressing metaplasia: reparative lineages in the gastrointestinal mucosa. *J Pathol* 2018;245:132–137.
  60. Herring CA, Banerjee A, McKinley, et al. Unsupervised trajectory analysis of single-cell RNA-seq and imaging data reveals alternative tuft cell origins in the gut. *Cell Syst* 2018;6:37–51.e9.
  61. Southard-Smith AN, Simmons AJ, Chen B, et al. Dual indexed library design enables compatibility of In-Drop single-cell RNA-sequencing with exAMP chemistry sequencing platforms. *BMC Genomics* 2020; 21:456.
  62. Lapierre LA, Manning EH, Mitchell KM, et al. Interaction of phosphorylated Rab11-FIP2 with Eps15 regulates apical junction composition. *Mol Biol Cell* 2017; 28:1088–1100.
- 
- Received October 12, 2023. Accepted May 20, 2024.**
- Correspondence**  
Address correspondence to: James R. Goldenring, MD, PhD, Epithelial Biology Center, Vanderbilt University Medical Center, 10435-G MRB IV, 2213 Garland Avenue, Nashville, Tennessee 37232. e-mail: jim.goldenring@vumc.org.
- CRedit Authorship Contributions**  
Ela Contreras Panta (Conceptualization: Lead; Data curation: Equal; Formal analysis: Lead; Investigation: Lead; Methodology: Equal; Validation: Lead; Visualization: Lead; Writing – original draft: Lead; Writing – review & editing: Equal)  
Su-Hyung Lee, DVM, PhD (Conceptualization: Equal; Data curation: Equal; Formal analysis: Lead; Investigation: Equal; Methodology: Equal; Validation: Equal; Visualization: Equal; Writing – original draft: Equal; Writing – review & editing: Equal)  
Yoonkyung Won, PhD (Resources: Equal; Validation: Equal; Writing – review & editing: Equal)  
Alison E. Norlander (Methodology: Supporting; Resources: Supporting; Writing – review & editing: Supporting)  
Allan J. Simmons (Data curation: Supporting; Formal analysis: Supporting; Investigation: Supporting; Writing – review & editing: Supporting)  
R. Stokes Peebles Jr, MD (Conceptualization: Supporting; Resources: Supporting; Writing – review & editing: Supporting)  
Ken S. Lau, PhD (Conceptualization: Supporting; Data curation: Supporting; Methodology: Supporting; Software: Supporting; Writing – review & editing: Supporting)  
Eunyoung Choi, PhD (Conceptualization: Supporting; Funding acquisition: Supporting; Methodology: Supporting; Project administration: Supporting; Resources: Supporting; Supervision: Supporting; Writing – review & editing: Supporting)  
James R. Goldenring, MD, PhD (Conceptualization: Equal; Funding acquisition: Lead; Investigation: Equal; Project administration: Lead; Resources: Supporting; Supervision: Lead; Writing – review & editing: Equal)
- Conflicts of interest**  
The authors disclose no conflicts.
- Funding**  
Supported by funding to James R. Goldenring from grants from a Department of Veterans Affairs Merit Review Award IBX000930, DOD CA190172, NIH R01 DK101332, and Cancer Research UK Grand Challenge Award 29075, and to Eunyoung Choi from grants from NIH R37 CA244970, R01 CA272687 and an AGA Research Foundation Funderburg Award (AGA2022-32-01). R. Stokes Peebles Jr is supported by VA Merit Review 2I01BX004299. Ken S. Lau is supported by P50CA236733, R01DK103831. The Vanderbilt Cell Imaging Shared Resource and the Vanderbilt Digital Histology Shared Resource are supported by the Vanderbilt Ingram Cancer Center (P30 CA068485) and the Vanderbilt Digestive Disease Research Center (P30 DK058404). The Translational Pathology Shared Resource is supported by NCI/NIH Cancer Center Support Grant (P30 CA68485). The Digital Histology Shared Resource is supported by VA Shared Equipment grant 1IS1BX003097 and the Vanderbilt Digestive Disease Research Center (P30 DK058404).